Bulletin of Mathematical Biology (2006)
DOI 10.1007/s11538-005-9016-1

ORIGINAL ARTICLE

Framework Models of Ion Permeation Through Membrane Channels and the Generalized King–Altman Method

Eric J. Mapes*, Mark F. Schumaker

Department of Mathematics, Washington State University, Pullman, WA 99164-3113, USA

Received: 21 July 2004 / Accepted: 3 March 2005

Abstract A modern approach to studying the detailed dynamics of biomolecules is to simulate them on computers. *Framework* models have been developed to incorporate information from these simulations in order to calculate properties of the biomolecules on much longer time scales than can be achieved by the simulations. They also provide a simple way to think about the simulated dynamics. This article develops a method for the solution of framework models, which generalizes the King–Altman method of enzyme kinetics. The generalized method is used to construct solutions of two framework models which have been introduced previously, the single-particle and Grotthuss (proton conduction) models. The solution of the Grotthuss model is greatly simplified in comparison with direct integration. In addition, a new framework model is introduced, generalizing the shaking stack model of ion conduction through the potassium channel.

Keywords Single-particle diffusion · Grotthuss conduction · Vacancy diffusion

1. Introduction

A modern approach to understanding the detailed dynamics of biomolecules is to simulate them on a computer (Roux, 2002; Roux et al., 2004). Molecular dynamics simulations integrate the laws of motion for a very large number of atoms in a detailed model of a biomolecule. Despite the rapidly increasing power of modern computers, there remains a very large gap in scales between the short time intervals over which direct molecular dynamics simulations can be made and the much longer time intervals often required to make comparisons with experiment. Even when such gaps in time scales are overcome by the advancement of computer technology, there will still be an important need to think about the dynamics in simple ways. One approach to overcoming the gap is to construct *framework*

*Corresponding author.
E-mail address: mapes@math.wsu.edu

models: Stochastic models designed to incorporate the potentials of mean force and diffusion coefficients estimated from the simulations (Schumaker et al., 2000; Bernèche and Roux, 2003). The potentials and diffusion coefficients are calculated as a function of reaction coordinates chosen as key degrees of freedom participating in the dynamics. These simplified models can then be used to make detailed comparisons with experiment (Gowen et al., 2002).

The framework models that we have constructed so far are models of ion permeation through membrane channels. They are also diffusion models. The diffusion approximation may ultimately be justified by a projection of high-dimensional Hamiltonian dynamics to a low-dimensional configuration space of slow variables (Zwanzig, 1961; Mori, 1965; Berne and Pecora, 1976; Zwanzig, 2001). The projection generally yields a generalized Langevin equation, an integro-differential equation. The influence of the other (fast) variables appears both as an additive "random force" and as a friction kernel in this equation. When there is a large gap in time scales between the slow and fast variables, the random force is often approximated by a Gaussian white noise and the friction kernel by a delta function. This yields a classical Langevin equation. Further, when the inertial term can be ignored, one obtains the diffusion approximation (Roux et al., 2004). In practice, the diffusion approximation is often assumed. This is true of the classical theory of ion permeation formulated by Goldman, Hodgkin, and Katz (Hille, 1992), Poisson–Nernst–Planck theory (for example, Chen et al., 1997) and Brownian Dynamics simulations of ion channels (for example, Allen and Chung, 2001; Mashl et al., 2001). However, the generalized Langevin equation is used by Grote–Hynes theory to calculate the rate of crossing over a parabolic potential barrier (Grote and Hynes, 1980). This has been applied to a model of the IRK1 potassium channel (Tolokh et al., 2002). The Brownian Dynamics technique can also be generalized to simulations of the sample paths of the generalized Langevin equation (Tuckerman and Berne, 1991).

The diffusing entity described by a framework model is the state of the system. For a model of ion permeation through a membrane channel, the state may correspond to a configuration of one or several ions within the channel pore. These models naturally incorporate experimental information about possible states of occupancy within the channel pore. An example of such evidence comes from X-ray crystallography—the selectivity filter (narrow part of the pore) of the KcsA potassium channel is usually occupied by two potassium ions (Morais-Cabral et al., 2001; Zhou and MacKinnon, 2004).

The Smoluchowski equation describes diffusion under the influence of a systematic force and diffusion coefficient. The framework models that are constructed below, solve the Smoluchowski equation directly under various conditions. Framework models can also be constructed by integrating the sample paths underlying the Smoluchowski equation using Brownian Dynamics. Bernèche and Roux (2003) give an excellent example, with both potential of mean force and diffusion coefficients obtained from molecular dynamics simulations. These quantities are estimated at the nodes of a rectangular grid and determine transition probabilities which depend on the potential of mean force and diffusion coefficients using a generalization of the Agmon–Hopfield expressions (Agmon and Hopfield, 1983). Schumaker and Watkins (2004) show that similar random walks

converge to the Smoluchowski equation as the distance between grid points goes to zero.

This article describes a systematic method of solving framework models whose configuration spaces involve only a single cycle of states. The cycle may include isolated states or continuous segments of states parameterized by single reaction coordinates. The method of solution is a generalization of the King–Altman method, which is popular within the enzyme kinetics community. The King–Altman method is based on solving a linear system of equations by Cramer's rule (King and Altman, 1956); however, traditional mathematical expressions are replaced by diagram expansions.

First, two framework models will be described in detail: The single-particle model and the Grotthuss model. Next, the original King–Altman method and its relationship with Cramer's rule are illustrated by a simple example. The generalized King–Altman method is then developed. Its use is demonstrated by calculating conductances and state probabilities for the single-particle and Grotthuss models. Finally, the generalized King–Altman method is used to construct a new framework model for ion conduction through the KcsA potassium channel.

2. Single-particle model

The gramicidin monomer is a peptide (a small protein) composed of 15 amino acids in a helical conformation (Arseniev et al., 1985; Ketcham et al., 1997). In biological membranes, the conducting form is a head-to-head dimer. The dimer has a cylindrical pore that is about 25 Å long and 4 Å in diameter. The pore is occupied by eight to ten water molecules in single file. Gramicidin allows small ions with a single positive charge to pass through the membrane; one of these permeant ions is sodium (Na^+). Three lines of argument, each based on conduction measurements and theoretical interpretation, suggest that only one Na^+ at a time can occupy the pore (Finkelstein and Andersen, 1981; Tripathi and Hladky, 1998). To our knowledge, boundary conditions that enforce the single-particle constraint were first proposed by Levitt (1986). McGill and Schumaker (1996) gave a systematic derivation of these by taking the diffusion limit of a random walk.

Figure 1(a) schematically portrays a gramicidin channel in a biological membrane occupied by a single ion. Waters are represented in the figure by angles with the electronegative oxygen at the vertex. One hydrogen participates in a bond with a backbone carbonyl and, in addition, water oxygens participate in hydrogen bonds with oxygens in front of and behind them. The waters coordinate with a helical backbone; the figure does not attempt to represent this geometry. A monovalent cation is represented by the circle with a plus sign. Simulations suggest that waters close to the cation are oriented with their electronegative oxygen close to the center of positive charge. Figure 1(b) shows the potential profile for Na^+ in gramicidin based on that calculated by Roux and Karplus (1993); z is the axial component of the ion's displacement from the pore center. The shape of the potential was calculated by molecular dynamics simulations but its amplitude was divided by 3 to

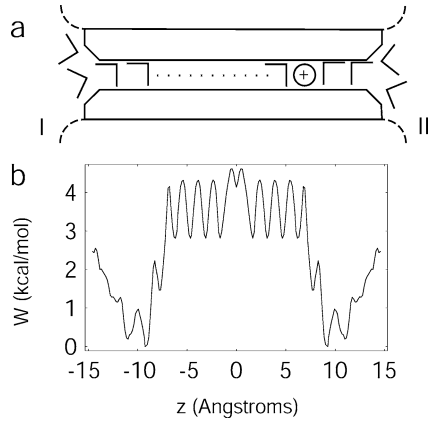

Fig. 1 (a) Schematic cross-section of a gramicidin channel in a biological membrane. (b) Scaled potential of mean force for Na^+ in gramicidin, based on the calculations of Roux and Karplus (1993).

give a better comparison with conductance data (McGill and Schumaker, 1996). In addition to the potential of mean force, effective diffusion coefficients as a function of the reaction coordinate can also be calculated from simulations (Chiu et al., 1993; Crouzy et al., 1994).

A state diagram for single-particle conduction is shown in Fig. 2(a). The horizontal line represents the states of the occupied pore, and is parameterized by the reaction coordinate ξ, which is a dimensionless variable corresponding to z in Fig. 1. The endpoint $\xi = 0$ corresponds to the ion at the channel entrance on side I, and the endpoint $\xi = 1$ corresponds to an ion at the channel entrance on side II. When the ion leaves the pore, the system makes a transition to the empty state E at the bottom of Fig. 2(a). Ion entrances correspond to transitions from E to the channel entrance at either end of the pore.

This state diagram may be constructed as the diffusion limit of the random walk depicted in Fig. 2(b). States $S_1, S_2, \ldots, S_n$ correspond to an ion in the pore, where in state S_i an ion is located at spatial coordinate $\xi_i = i/n$, $1 \leq i \leq n$. The letter

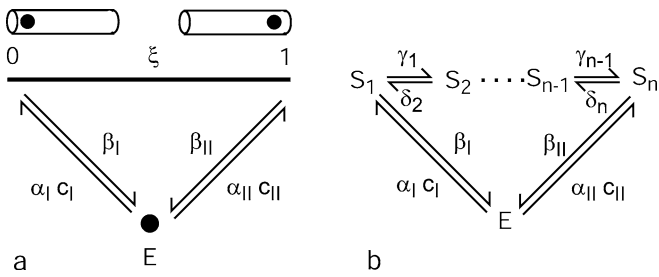

Fig. 2 (a) State diagram for the single-particle model. (b) State diagram of the random walk used to construct the single-particle model.

E corresponds to an empty pore, that is, a pore occupied only by water. By the construction of the random walk, the pore is either empty or occupied by a single walker. It is manifest that, when we take the diffusion limit $n \to \infty$, the resulting process will describe a pore that is either empty or occupied by a single diffuser.

Symbols for the transition rates between the states of the random walk in Fig. 2(b) are given above and below the arrows. These rates are defined by:

$$\gamma_i = t_D^{-1} n^2 d_{i,i+1}\, \mathrm{e}^{[w(\xi_i)-w(\xi_{i+1})]/2}, \tag{1}$$

$$\delta_i = t_D^{-1} n^2 d_{i,i-1}\, \mathrm{e}^{[w(\xi_i)-w(\xi_{i-1})]/2}, \tag{2}$$

$$\alpha_{\mathrm{I}} c_{\mathrm{I}} = t_D^{-1} \kappa_{\mathrm{I}}^{-1} v_0\, \mathrm{e}^{\psi_1 - w(0)} c_{\mathrm{I}}, \tag{3}$$

$$\beta_{\mathrm{I}} = t_D^{-1} \kappa_{\mathrm{I}}^{-1} n, \tag{4}$$

$$\alpha_{\mathrm{II}} c_{\mathrm{II}} = t_D^{-1} \kappa_{\mathrm{II}}^{-1} v_0\, \mathrm{e}^{-w(1)} c_{\mathrm{II}}, \tag{5}$$

$$\beta_{\mathrm{II}} = t_D^{-1} \kappa_{\mathrm{II}}^{-1} n. \tag{6}$$

The rate of ion entry into the channel from the bulk solution on side R is $\alpha_R c_R$, where $R \in \{\mathrm{I}, \mathrm{II}\}$. The rate of ion exit from the channel into the bulk solution is β_R. In the occupied state, $\gamma_i, 1 \le i \le n-1$, is the rate of moving in the direction of higher indices from site i and $\delta_i, 2 \le i \le n$, is the rate of moving in the direction of lower indices from site i.

Transition rates between the occupied states, Eqs. (1) and (2), have the form introduced by Agmon and Hopfield (1983). The transition rates used by Apaydin et al. (2003) in their random walk model of protein folding also depend exponentially on energy differences. We use the generalization of the Agmon–Hopfield form introduced by Bernèche and Roux (2003), which yields a Smoluchowski equation with state-dependent diffusion coefficients when the diffusion limit is taken. The symbol $d_{i,j}$ represents the mean diffusivity $(d_i + d_j)/2$ where $d_i = D_i/D_0$. D_i is the diffusion coefficient associated with site i and d_i is the corresponding dimensionless value. A diffusion scale D_0 is introduced. t_D is the diffusion time scale; for a channel of length L and diffusion coefficient D_0, $t_D = L^2/D_0$. t_D has units of time and the other quantities represented on the right-hand side of Eqs. (1)–(6) are dimensionless. $w(\xi) = W/(k_{\mathrm{B}}T)$ is a dimensionless potential of mean force, where W is the potential with units of energy, k_{B} is Boltzmann's constant, and T is the absolute temperature.

The particle entrance rates, $\alpha_R c_R$, are independent of n. This means that the distribution of entrances into the channel is exponential, and does not change in the diffusion limit $n \to \infty$. The exponential distribution is a reasonable first approximation for the distribution of empty state dwell times. Physically, the exponential distribution refers to entrances associated with distinct particles. It does not capture the highly correlated motions of a single particle, which may cross an arbitrary threshold several times in the process of entering a pore. The exponential distribution of distinct arrivals by noninteracting diffusers has been rigorously established (Nadler et al., 2001). The constants κ_R, $R \in \{\mathrm{I}, \mathrm{II}\}$, are proportional to access resistance on side R, and may be regarded as controlling the mean time before ion

entrance into the channel from side R. $\psi_{\mathrm{I}} = \Psi_{\mathrm{I}}/(k_{\mathrm{B}}T)$ is the dimensionless applied potential on side I, modeling an electrical potential difference between the two sides of the membrane (the applied potential on side II is zero by convention). $c_R = C_R/C_\bullet$ is the dimensionless ion concentration on side R. C_R is the ion concentration in standard units and $C_\bullet$ is the standard unit concentration, e.g., 1 M. v_0 is a dimensionless pore volume.

The exit rates, β_{I} and β_{II}, are proportional to n. This can be understood from the requirement that the particle flux from the empty state into an entrance must equal the flux from the same entrance back into the empty state at thermodynamic equilibrium (the condition of *detailed balance*). The probability of the empty state, Q_E, remains finite and positive as $n \to \infty$, and thus $Q_E \alpha_R c_R$ does too. In the diffusion limit, the probabilities of the states representing the occupied channel scale as n^{-1} (so that the total probability of the occupied state remains positive and finite). Thus, the exit rates must be proportional to n in order that the exit fluxes, $Q_1\beta_{\mathrm{I}}$ and $Q_n\beta_n$, remain finite and positive as $n \to \infty$.

We now take the diffusion limit of the random walk shown in Fig. 2(b), with transition rates defined by Eqs. (1)–(6), to obtain the single-particle model. Let Q_i, for $1 \le i \le n$, be the probability that the random walker will be at S_i, an occupied state of the channel in Fig. 2(b). At any steady state, the flow of probability into S_i equals the flow out. Hence, for $2 \le i \le n-1$, we have

$$Q_i(\delta_i + \gamma_i) = Q_{i-1}\gamma_{i-1} + Q_{i+1}\delta_{i+1}. \tag{7}$$

To obtain the time-independent Smoluchowski equation, put

$$Q_i = p_i \Delta\xi, \tag{8}$$

where $p_i = p(\xi_i)$ converges to a probability density at ξ_i as $n \to \infty$. $\Delta\xi = n^{-1}$ is the distance between two adjacent sites. Expand γ_i and δ_i in Taylor series:

$$\gamma_i = t_D^{-1} n^2 d_{i,i+1}[1 - w_i' n^{-1}/2 + \epsilon_i n^{-2} + O(n^{-3})], \tag{9}$$

$$\delta_i = t_D^{-1} n^2 d_{i,i-1}[1 + w_i' n^{-1}/2 + \epsilon_i n^{-2} + O(n^{-3})], \tag{10}$$

where $w_i = w(\xi_i)$, $w_i' = w'(\xi_i)$, etc., with

$$\epsilon_i = -w_i''/4 + (w_i')^2/8. \tag{11}$$

Substitute Eqs. (8) through (10) into Eq. (7) and let $n \to \infty$ to obtain, after some algebra

$$(d(\xi)p'(\xi))' + (d(\xi)w'(\xi)p(\xi))' = 0. \tag{12}$$

Equation (12) may be integrated once to obtain the Nernst–Planck equation:

$$J = -t_D^{-1} d(\xi)[p'(\xi) + w'(\xi)p(\xi)] \tag{13}$$

where the constant of integration, J, is the probability current. Alternately, we may use the following useful formula:

$$J = \lim_{n\to\infty} (Q_i\gamma_i - Q_{i+1}\delta_{i+1}). \tag{14}$$

The Nernst–Planck equation is easily obtained by substituting from Eqs. (8) through (10) and letting $n \to \infty$.

The first term on the right of the Nernst–Planck equation is the contribution of Fick's law, which, by itself, would describe a steady probability current flowing down a concentration gradient. The second term models the influence of the potential energy w; probability tends to flow downhill in the direction of $-w'$. A positive current J corresponds to flow in the direction of increasing values of the independent variable ξ, which is clockwise around the state diagram of Fig. 2(a).

The point of the random walk construction of the single-particle model is to obtain boundary conditions for the Smoluchowski equation that enforce the single-particle constraint. To obtain the boundary condition on side I, balance probability flowing into and out of site S_1 in Fig. 2(b):

$$Q_1(\beta_\mathrm{I} + \gamma_1) = Q_E\alpha_1 c_\mathrm{I} + Q_2\delta_2. \tag{15}$$

Substitute from Eqs. (3), (4), and (8) and let $n \to \infty$, using (14). The analysis on side II is similar. Obtain

$$p(0) = Q_E v_0\, \mathrm{e}^{\psi_1 - w(0)} c_\mathrm{I} - J t_D \kappa_\mathrm{I}, \tag{16}$$

$$p(1) = Q_E v_0\, \mathrm{e}^{-w(1)} c_\mathrm{II} + J t_D \kappa_\mathrm{II}. \tag{17}$$

Since the system must be in some state in Fig. 2(a), we normalize

$$Q_E + \int_0^1 p(\xi)\,\mathrm{d}\,\xi = 1. \tag{18}$$

The boundary conditions, Eqs. (16) and (17), are somewhat unusual because, through the factor Q_E, they refer to the solution $p(\xi)$ in the interior of its domain $[0, 1]$, and not just at the endpoints. They are an example of *nonlocal* boundary conditions. For κ_I, $\kappa_\mathrm{II} > 0$, we call them *exponential* boundary conditions (Schumaker, 2002) because they correspond to exponentially distributed waiting times in the empty state. Yin (2004) has obtained the existence and uniqueness of solutions to a class of Smoluchowski equations with nonlocal boundary conditions similar to the single-particle model.

A modified formulation of the random walk construction does not lead to exponentially distributed entrances, but instead to the single-particle boundary conditions originally proposed by Levitt (1986). To obtain Levitt's boundary conditions, retain the definitions of the transition rates between sites S_i and S_j, Eqs. (1) and (2). Transition rates corresponding to ion entrance and exit, Eqs. (3)–(6), are each multiplied by n (McGill and Schumaker, 1996). Repeating the derivation of the boundary conditions, obtain Eqs. (16) and (17) with $\kappa_\mathrm{I} = \kappa_\mathrm{II} = 0$. The mean time in the empty state in Levitt's model is zero. In the single-particle model that

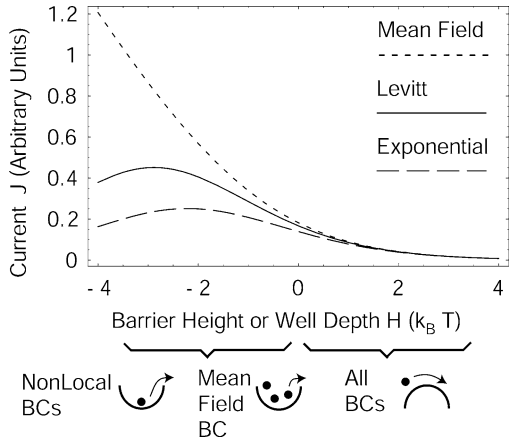

Fig. 3 Current as a function of parabolic barrier height H: $C_{\mathrm{I}} = 1\mathrm{M}$, $C_{\mathrm{II}} = 0$, and $\Psi_{\mathrm{I}} = 0$. When $H < 0$, the potential is a parabolic energy well. Cartoons below the graph indicate the qualitative nature of trajectories for $H < 0$ and $H > 0$.

uses the entrance rates defined by Eqs. (3) and (5), the mean time in the empty state is positive and the constants κ_{I} and κ_{II} are proportional to access resistance (Schumaker, 2002). This is the electrical resistance of the bulk medium outside the channel to ions diffusing from infinity to the channel entrance. Levitt's boundary conditions do not include a model for access resistance.

In the cases of both exponential and Levitt boundary conditions, Eqs. (13) and (16)–(18) may be integrated directly to obtain expressions for J, Q_E, and $p(\xi)$ (McGill and Schumaker, 1996; Schumaker, 2002). Solutions for both cases, and a third described below, are shown in Fig. 3. To construct this figure, the potential $w(\xi)$ is assumed to be a parabolic energy barrier of height H. When $H < 0$, the potential is instead an energy well.

The solid curve of Fig. 3 shows the single-particle model with Levitt's original boundary conditions, corresponding to Eqs. (16) and (17) with $\kappa_{\mathrm{I}} = \kappa_{\mathrm{II}} = 0$. These boundary conditions incorporate no model of access resistance. Physically, the current decreases as $H > 0$ increases because less current passes over an increasingly high energy barrier. The current decreases as $H < 0$ decreases because it becomes increasingly difficult for the occupying particle to escape the energy well. The long-dashed curve shows the single-particle model with exponential boundary conditions, corresponding to Eqs. (16) and (17) with $\kappa_{\mathrm{I}} = \kappa_{\mathrm{II}} > 0$, modeling access resistance (Schumaker, 2002). When $H > 0$, diffusion over the parabolic energy barrier is rate limiting and solutions for the exponential and Levitt boundary conditions nearly coincide. When $H < 0$, however, the current for exponential boundary conditions is less than that for Levitt boundary conditions. This is because the terms proportional to κ_{I} and κ_{II} slow both entrance and exit of trajectories from the interval $0 \leq \xi \leq 1$.

To develop an understanding of the effect of the nonlocal factor Q_E, consider the solution of Eq. (12) with boundary conditions given by Eqs. (16) and (17), except that Q_E is replaced by 1 (Schumaker, 2002). This is given by the

short-dashed curve in Fig. 3. To make this comparable to the solid curve we also put $\kappa_{\mathrm{I}} = \kappa_{\mathrm{II}} = 0$. This short-dashed curve departs from the single-particle theory for $H < 0$. Replacing $Q_E \to 1$ in the boundary conditions gives a *mean field theory*. Schumaker (2002) constructs the trajectories underlying this theory as a sum of single-particle processes. Any number of particles can now occupy the pore, as indicated by the cartoon below the graph in Fig. 3. As the energy well becomes deeper, it simply fills up with more particles. The current then increases as H becomes more negative. Goldman–Hodgkin–Katz theory (Hille, 1992) and Poisson–Nernst–Planck theory as described by Chen et al. (1997) have similar mean field boundary conditions.

3. Grotthuss conduction model

Proton transport in aqueous solution is different than the diffusion of other species since, in order for a net proton to move from one spatial location to another, no single proton need move through distances much greater than the average separation between water molecules. Only the bonds between hydrogens and oxygens need be rearranged. This is called Grotthuss conduction (Agmon, 1995). In view of the difference in mechanism, it is not surprising that proton transport may be much more rapid than transport of other ions. The framework model introduced in this section is an elaboration of the single-particle model because it describes the reorientation of water molecules in the empty state. For ions such as Na^+ the reorientation step is much faster than others required for permeation, so reorientation need not be included in their framework models. An experimentally accessible model of proton transport along a single file of water molecules is provided by proton conduction through gramicidin (Eisenman et al., 1980). This has been simulated by molecular dynamics (Pomès and Roux, 1996, 2002) and the Grotthuss model was constructed to compare the results with conductance measurements (Schumaker et al., 2000, 2001; Gowen et al., 2002).

Figure 4 depicts a simplified configuration space for single-proton conduction in gramicidin. The top line segment represents the states of a pore occupied by a single excess proton, and is parameterized by ξ^H. The proton can move from one end of the pore to the other, as depicted by the cartoons above. As the charge moves, hydrogen bonds reform so that water dipoles are in an energetically favorable conformation. If the proton leaves the pore on the right, the water column will be left partially ordered, with the electronegative oxygens oriented towards the center of excess positive charge on the right. However, waters may be partially disordered, especially near side I. The bottom line segment represents the states of an *empty* pore (without an excess charge), and is parameterized by ξ^E. The pair of dashed lines to the right indicates a range of possible transitions that can be made from the occupied segment to a subinterval of states on the empty segment called boundary region II. This range of transitions models a range of possible disordered states of the water column after ion exit. A similar range of transitions is shown on the left, associated with boundary region I. Potential of mean force calculations for the occupied and empty pores are shown in Fig. 4(b) and (c), respectively (Gowen et al., 2002; Pomès and Roux, 2002).

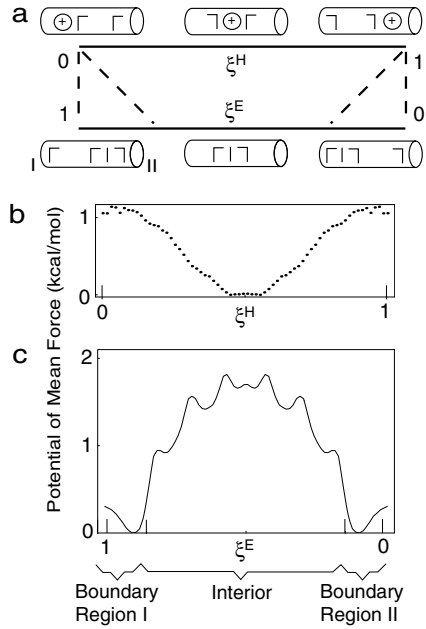

Fig. 4 (a) Simplified configuration space for single-proton conduction in gramicidin. (b) Proton potential of mean force (Pomès and Roux, 2002). (c) Water reorientation potential of mean force, with amplitude reduced to be consistent with conductance data from gramicidin A and two analogs (Gowen et al., 2002).

Figure 5(a) shows a state diagram for the framework model of single-proton conduction. Each filled circle represents a boundary region indicated in Fig. 4(a), but lumped to give an analytically soluble model. The lumped state approximation gives accurate mean first passage times across the empty pore segment if the central barrier is sufficiently high and the boundary regions are not too wide (Mapes and Schumaker, 2001). Currents computed using the analytical model (from Eqs. (28)–(33) given later) are in excellent agreement with a numerical calculation that avoids the lumped state approximation (Schumaker, 2003).

The random walk depicted in Fig. 5(b) is used to construct the state diagram for single-proton conduction. States H_i correspond to a proton in the pore at $\xi^H = i/n$ and states E_i correspond to an empty pore at $\xi^E = i/n$. The following transition rates generalize the model of Gowen et al. (2002) by including terms that yield state-dependent diffusion coefficients:

$$\gamma_i^s = t_s^{-1} n^2 d_{i,i+1}^s \, \mathrm{e}^{[w^s(\xi_i) - w^s(\xi_{i+1})]/2}, \tag{19}$$

$$\delta_i^s = t_s^{-1} n^2 d_{i,i-1}^s \, \mathrm{e}^{[w^s(\xi_i) - w^s(\xi_{i-1})]/2}, \tag{20}$$

$$\alpha_{\mathrm{I}} c_{\mathrm{I}} = t_a^{-1} a^{-1} \, \mathrm{e}^{\zeta + f_N \psi_{\mathrm{I}}} c_{\mathrm{I}}, \tag{21}$$

$$\beta_{\mathrm{I}} = t_a^{-1} n \, \mathrm{e}^{-f_X \psi_{\mathrm{I}}}, \tag{22}$$

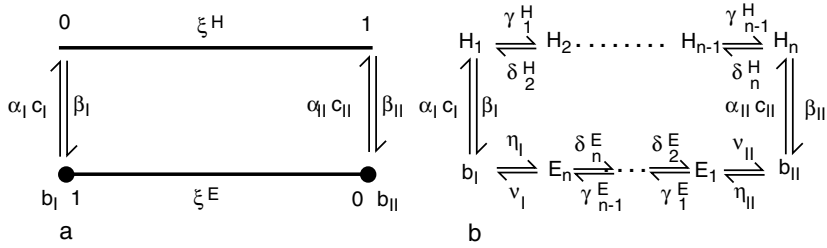

Fig. 5 (a) State diagram for the single-proton conduction model. Each *filled circle* on the bottom segment represents a boundary region of the configuration space shown in Fig. 4a. (b) Random walk used to construct the state diagram for the single-proton conduction model.

$$\alpha_{\mathrm{II}} c_{\mathrm{II}} = t_a^{-1} a^{-1} \, \mathrm{e}^{\zeta - f_N \psi_{\mathrm{I}}} c_{\mathrm{II}}, \tag{23}$$

$$\beta_{\mathrm{II}} = t_a^{-1} n \, \mathrm{e}^{f_X \psi_{\mathrm{I}}}, \tag{24}$$

$$\nu_{\mathrm{I}} = t_E^{-1} n^2 a \, \mathrm{e}^{f_B \psi_{\mathrm{I}}}, \tag{25}$$

$$\eta_{\mathrm{I}} = \eta_{\mathrm{II}} = t_E^{-1} n, \tag{26}$$

$$\nu_{\mathrm{II}} = t_E^{-1} n^2 a \, \mathrm{e}^{-f_B \psi_{\mathrm{I}}}, \tag{27}$$

where $s = H$ (proton) or $s = E$ (empty). γ_i^s, for $1 \le i \le n$, is the rate of moving forward (clockwise around the diagram), and δ_i^s, for $1 \le i \le n$, is the rate of moving backward (counterclockwise). $\alpha_R c_R$ and β_R, respectively, give the rate of excess proton entry into the pore and escape from the pore on side R. ν_R and η_R are rates of transitions between the empty segment and the lumped states.

The mean diffusivity $d_{i,j}^s = (d_i^s + d_j^s)/2$ where $d_i^s = D_i^s / D_0$, where D_i^s is the diffusion coefficient associated with site s_i and D_0 is the diffusion scale. w^s is the potential of mean force, ψ_{I} is the applied electrical potential on side I, and t_s is the time constant associated with segment s. The access time t_a is the time constant associated with proton entrance and exit. c_R is the concentration of excess protons in the bulk solution on side $R \in \{\mathrm{I}, \mathrm{II}\}$. The parameter ζ is a real number, a is a positive real number, and f_B, f_N, and f_X are positive or zero. Their physical interpretations are given by Schumaker et al. (2001) and Gowen et al. (2002). All quantities in the definitions for the transition rates are dimensionless except for the time constants.

As with the single-particle model, ordinary differential equations, boundary conditions, and a normalization condition are obtained by balancing the flow of probability into and out of appropriate states, similar to Eq. (7), and taking the limit $n \to \infty$. One obtains (Schumaker et al., 2001; Gowen et al., 2002):

$$(d^s(\xi^s) p^{s\prime}(\xi^s))' + (d^s(\xi^s) w^{s\prime}(\xi^s) p^s(\xi^s))' = 0 \quad \text{for } s \in \{H, E\}, \tag{28}$$

$$Q_{\mathrm{I}}^b = p^E(1) a \, \mathrm{e}^{f_B \psi_{\mathrm{I}}}, \tag{29}$$

$$Q_{\mathrm{II}}^b = p^E(0) a \, \mathrm{e}^{-f_B \psi_{\mathrm{I}}}, \tag{30}$$

$$p^H(0)\,\mathrm{e}^{-f_X\psi_1} = Q_{\mathrm{I}}^b a^{-1}\,\mathrm{e}^{\zeta+f_N\psi_1}c_{\mathrm{I}} - Jt_a, \tag{31}$$

$$p^H(1)\,\mathrm{e}^{f_X\psi_1} = Q_{\mathrm{II}}^b a^{-1}\,\mathrm{e}^{\zeta-f_N\psi_1}c_{\mathrm{II}} + Jt_a, \tag{32}$$

$$\int_0^1 p^E(\xi^E)\,\mathrm{d}\,\xi^E + \int_0^1 p^H(\xi^H)\,\mathrm{d}\,\xi^H + Q_{\mathrm{I}}^b + Q_{\mathrm{II}}^b = 1. \tag{33}$$

In these equations, $p^s(\xi^s)$ is a probability density on segment s and Q_R^b is the probability of the lumped state b_R. The net current clockwise around the diagram is J. Equations (28) are obtained by balancing probability about the state i, $2 \le i \le n-1$, on segment s. Equations (29) and (30) are obtained by balancing probability about states b_{I} and b_{II}, respectively. Equations (31) and (32) are obtained by balancing probability about the states H_1 and H_n, respectively. Equation (14), applied to states on segment s, is used to obtain the terms proportional to J. Equation (33) normalizes probability.

Analytical solutions of the Grotthuss model are important because a thorough comparison with experimental data involves a very large number of current evaluations. For example, the sensitivity analysis of Gowen et al. (2002) involved over a million evaluations. Each evaluation involves the solution of the model for different parameter values or under a different set of experimental conditions. They can be performed extremely quickly when they are based on an analytical solution. A special case of Eqs. (28)–(33) has been solved by direct integration (Schumaker et al., 2001). The calculations are straightforward, but lengthy. The King–Altman Method, which we introduce next, will be generalized to provide a much less tedious method for finding the solution.

4. The generalized King–Altman method

4.1. The King–Altman method

The King–Altman method (King and Altman, 1956; Hill, 1977) is a diagrammatic method for finding the steady-state solutions of Markov chains. An important element of this method is the *directed diagram*. In the terminology of graph theory, this is a spanning tree graph with every edge directed towards some fixed vertex. The product of transition rates corresponding to each edge is represented by the diagram. An example is shown in Fig. 6(a). All transitions are directed towards state E, and the diagram represents the product $\gamma_1 \times \cdots \times \gamma_{n-1}\beta_{\mathrm{II}}$.

To illustrate the steady-state solution of a Markov chain, consider the three-state diagrams shown in Fig. 6(b). The transition rate from site i to site j is denoted k_{ij}. Let the probability of state i be denoted Q_i. Then, the steady state is the solution of

$$\begin{pmatrix} -(k_{12}+k_{13}) & k_{21} & k_{31} \\ k_{12} & -(k_{21}+k_{23}) & k_{32} \\ 1 & 1 & 1 \end{pmatrix} \begin{pmatrix} Q_1 \\ Q_2 \\ Q_3 \end{pmatrix} = \begin{pmatrix} 0 \\ 0 \\ 1 \end{pmatrix}. \tag{34}$$

The first two equations balance the flow of probability into and out of states 1 and 2. The equation balancing the flow of probability into and out of state 3

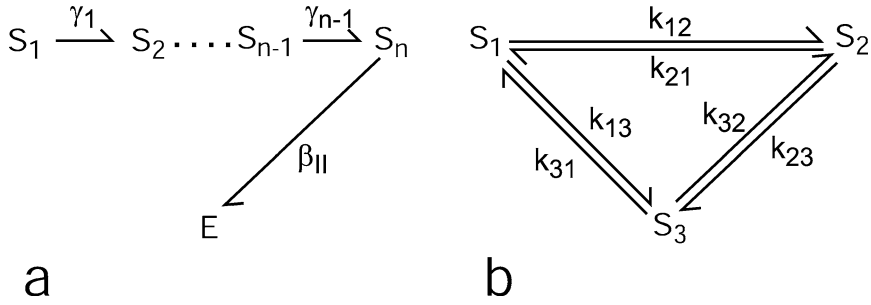

Fig. 6 (a) A *directed diagram* of the original King–Altman method; this diagram is an element of the solution of the steady-state probabilities of the Markov chain depicted in Fig. 2(b). (b) A three-state Markov chain.

is a linear combination of these and is omitted. The last equation normalizes probability.

Let A be the matrix and let **b** be the column vector on the right-hand side of Eq. (34). Then, according to Cramer's rule, $Q_i = \det(B_i)/\det(A)$, where B_i is the matrix obtained by replacing the ith column of A by **b**. Representing products of transition rates by directed diagrams, the solution can be written

$$\mathcal{D}Q_1 = \quad + \quad + \quad ,$$
$$\mathcal{D}Q_2 = \quad + \quad + \quad ,$$
$$\mathcal{D}Q_3 = \quad + \quad + \quad , \tag{35}$$

where $\mathcal{D} = \mathcal{D}Q_1 + \mathcal{D}Q_2 + \mathcal{D}Q_3 = \det(A)$ is the sum of all of the directed diagrams. King and Altman (1956) show that, in general, the probability of state i is equal to the sum of all diagrams directed towards state i divided by the sum of all directed diagrams. Hill (1977) gives an interesting alternative proof of the validity of this method that does not refer to Cramer's rule.

The net flux J clockwise around the cycle is given by

$$J = Q_1 k_{12} - Q_2 k_{21}$$
$$= \Big(\quad 1 \quad 2 \quad 3 \quad - \quad 1 \quad 2 \quad 3 \quad \Big) \tag{36}$$

where the last expression is obtained after a cancellation of terms. This evocative difference between diagrams is easy to remember and appeals to biophysicists. The same structure is preserved in the generalized method introduced later.

4.2. *Construction of the generalized King–Altman dictionary*

We have constructed the single-particle and Grotthuss framework models by taking the diffusion limit of random walks. From these limits we obtained the Smoluchowski equation on intervals of states, boundary conditions, and normalization conditions. These boundary value problems may be solved directly. However, we will show that the framework models are also solved by the limits of the solutions of the random walks. This section demonstrates the construction of several components of those limits, which will be entries in a dictionary give in Section 4.3.

Similar to the original King–Altman method, state probabilities calculated by the generalized method will always be expressed as a limit of a ratio of directed diagrams. The ratio will have the form

$$Q = \frac{\mathcal{D}Q}{\mathcal{D}} \tag{37}$$

where $\mathcal{D}Q$ is a sum of directed diagrams directed towards state Q and $\mathcal{D}$ is the sum of all directed diagrams. Each directed diagram is a positive product of transition rates. The numerator and denominator of Eq. (37) will therefore be sums of positive terms. Since all of the terms in the numerator are also found in the denominator, the leading power of n in the denominator will always be equal to, or greater than, the leading power of n in the numerator. If the numerator and denominator are divided by the leading power of n in the denominator, the numerator will converge to a finite limit and the denominator will converge to a finite, positive, limit as $n \to \infty$. Our dictionary entries will enter into the expressions for $\mathcal{D}Q$ and $\mathcal{D}$ in state probabilities with the form of Eq. (37). We are therefore free to simplify the entries by taking the limit $n \to \infty$ of certain of their components so long as these limits exist. The elementary limit laws of calculus guarantee that we can use these simplified entries to form simplified ratios, following the pattern of Eq. (37), then divide through by the leading power of n in the denominator, and finally take a simplified final limit $n \to \infty$ to calculate state probabilities by the generalized method.

To construct the first term of the dictionary, consider the random walk depicted in Fig. 2(b). State S_i is located at $\xi_i = i/n$. The random walk on the states $\{S_1, \ldots, S_n\}$ converges to a diffusion on the interval $[0, 1]$ as $n \to \infty$. From Eq. (1), the product of transition rates from S_1 to S_n is

$$\begin{aligned} \overset{1}{\bullet}\xrightarrow{\gamma_1}\bullet\cdots\bullet\xrightarrow{\gamma_{n-1}}\overset{n}{\bullet} &= \prod_{i=1}^{n-1} t_D^{-1} n^2 d_{i,i+1} \mathrm{e}^{[w(\xi_i)-w(\xi_{i+1})]/2} \\ &= F\mathrm{e}^{[w(\xi_1)-w(\xi_n)]/2}, \end{aligned} \tag{38}$$

where

$$F = t_D^{-(n-1)} n^{2(n-1)} \prod_{i=1}^{n-1} d_{i,i+1}. \tag{39}$$

The dictionary entry can be simplified slightly by taking the limit $n \to \infty$ only in the exponent of Eq. (38). Define γ:

$$\gamma = F\,\mathrm{e}^{[w(0)-w(1)]/2}. \tag{40}$$

We will often consider such a product of transition rates with increasing index on a segment of a state diagram that will model diffusion. γ is the first entry of our dictionary of directed diagrams for the generalized King–Altman method.

Now consider only those transitions within states $\{S_1, \ldots, S_n\}$ that are directed towards a particular site i, $1 \le i \le n$, in the interval. The diagram depicting these and the associated product of rates is

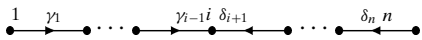

$$= \gamma_1 \cdots \gamma_{i-1} \cdot \delta_{i+1} \cdots \delta_n$$
$$= F\,\mathrm{e}^{[w(\xi_1)-2w(\xi_i)+w(\xi_n)]/2}. \tag{41}$$

Again, let $n \to \infty$ in the exponent to define the symbol

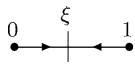

$$= F\,\mathrm{e}^{[w(0)-2w(\xi)+w(1)]/2}, \tag{42}$$

where $\xi_1 \to 0$, $\xi_n \to 1$, and $\xi_i \to \xi$ as $n \to \infty$. The solid vertical line represents ξ, the value to which the arrows converge. We next sum Eq. (41) over site i:

$$\sum_{i=1}^{n}$$ 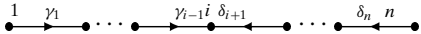

$$= F\mathrm{e}^{[w(\xi_1)+w(\xi_n)]/2} \sum_{i=1}^{n} \mathrm{e}^{-w(\xi_i)}. \tag{43}$$

Multiply the right-hand side by $\Delta\xi/\Delta\xi$ where $\Delta\xi = 1/n$. The factor of $\Delta\xi$ in the numerator is used to construct a Riemann sum. Letting $n \to \infty$ in the exponents and sum, we define

$$\int_0^1$$ 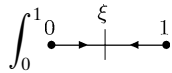

$$\mathrm{d}\,\xi = Fn\,\mathrm{e}^{[w(0)+w(1)]/2} \int_0^1 \mathrm{e}^{-w(\xi)}\,\mathrm{d}\,\xi. \tag{44}$$

Note that the right-hand side of Eq. (44) is obtained from the right-hand side of Eq. (42) by integrating with respect to ξ and multiplying by n.

We next consider only transitions within states $\{S_1, \ldots, S_n\}$ that are directed away from a missing link between sites i and $i+1$. The diagram and associated product of rates is:

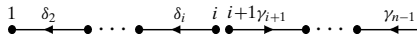

$$= \delta_2 \cdots \delta_i \cdot \gamma_{i+1} \cdots \gamma_{n-1}$$
$$= Ft_D n^{-2} \mathrm{e}^{[-w(\xi_1)+w(\xi_i)+w(\xi_{i+1})-w(\xi_n)]/2} d_{i,i+1}^{-1}. \tag{45}$$

Take the limit $n \to \infty$ in the exponent, where both ξ_i and $\xi_{i+1} \to \xi'$ and $d_{i,i+1} \to d(\xi')$, to define

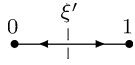

$$= Ft_D n^{-2}\,\mathrm{e}^{-[w(0)-2w(\xi')+w(1)]/2} d(\xi')^{-1}. \tag{46}$$

The dashed vertical line represents ξ', the value from which the arrows diverge. Next, sum both sides of Eq. (45) over all possible missing links to give

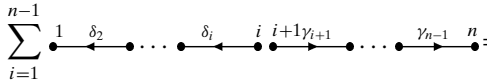

$$= Ft_D n^{-2}\, \mathrm{e}^{-[w(\xi_1)+w(\xi_n)]/2} \times \sum_{i=1}^{n-1} \mathrm{e}^{1/2[w(\xi_i)+w(\xi_{i+1})]} d_{i,i+1}^{-1}. \tag{47}$$

Multiply the right side by $\Delta\xi/\Delta\xi$, using the factor of $\Delta\xi$ in the numerator to construct a Riemann sum. Let $n \to \infty$ in the Riemann sum and the exponent to give

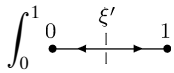

$$\mathrm{d}\,\xi' = Ft_D n^{-1}\, \mathrm{e}^{-[w(0)+w(1)]/2} \int_0^1 \mathrm{e}^{w(\xi')} d(\xi')^{-1}\, \mathrm{d}\,\xi'. \tag{48}$$

We finally consider transitions within states $\{S_1, \ldots, S_n\}$ that are directed towards a site i and away from a missing link between sites j and $j+1$, with $i < j$. The diagram and associated products of rates is

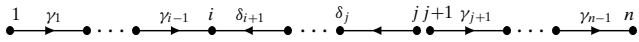

$$= Ft_D n^{-2}\, \mathrm{e}^{[w(\xi_1)-2w(\xi_i)+w(\xi_j)+w(\xi_{j+1})-w(\xi_n)]/2} d_{j,j+1}^{-1}. \tag{49}$$

Take the limit $n \to \infty$ in the exponent, where $\xi_i \to \xi$ and both ξ_j and $\xi_{j+1} \to \xi'$. In addition $d_{j,j+1} \to d(\xi')$ as $n \to \infty$. Define

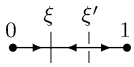

$$= Ft_D n^{-2}\, \mathrm{e}^{[w(0)-2w(\xi)+2w(\xi')-w(1)]/2} d(\xi')^{-1}. \tag{50}$$

Next, sum both sides of Eq. (49) over all possible missing links to give

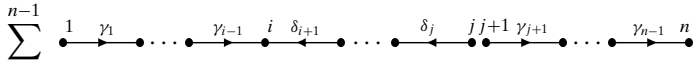

$$= Ft_D n^{-2}\, \mathrm{e}^{[w(\xi_1)-2w(\xi_i)-w(\xi_n)]/2} \sum_{j=i}^{n-1} \mathrm{e}^{[w(\xi_j)+w(\xi_{j+1})]/2} d_{j,j+1}^{-1}. \tag{51}$$

Multiply the right side by $\Delta\xi/\Delta\xi$, using the factor of $\Delta\xi$ in the numerator to construct a Riemann sum. Let $n \to \infty$ in the Riemann sum and the exponent to give

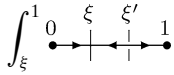

$$\mathrm{d}\,\xi' = Ft_D n^{-1}\, \mathrm{e}^{[w(0)-2w(\xi)-w(1)]/2} \int_\xi^1 \mathrm{e}^{w(\xi')} d(\xi')^{-1} \mathrm{d}\,\xi'. \tag{52}$$

Summing Eq. (51) over i, we obtain

$$\sum_{i=1}^{n-1}\sum_{j=i}^{n-1} \quad \underset{1}{\bullet}\xrightarrow{\gamma_1}\cdots\xrightarrow{\gamma_{i-1}}\underset{i}{\bullet}\xleftarrow{\delta_{i+1}}\cdots\xleftarrow{\delta_j}\underset{j}{\bullet}\xrightarrow{\gamma_{j+1}}\underset{j+1}{\bullet}\cdots\xrightarrow{\gamma_{n-1}}\underset{n}{\bullet}$$

$$= Ft_D n^{-2}\,\mathrm{e}^{[w(\xi_1)-w(\xi_n)]/2}\sum_{i=1}^{n-1}\sum_{j=i}^{n-1}\mathrm{e}^{[-2w(\xi_i)+w(\xi_j)+w(\xi_{j+1})]/2}d_{j,j+1}^{-1}. \tag{53}$$

Multiply the right side by $\Delta\xi^2/\Delta\xi^2$, using the factor of $\Delta\xi^2$ in the numerator to construct a Riemann sum. Let $n\to\infty$ in the Riemann sum and the exponent to give

$$\int_0^1\int_\xi^1 \underset{0}{\bullet}\xrightarrow{\quad}\underset{\xi}{|}\xrightarrow{\quad}\underset{\xi'}{|}\xrightarrow{\quad}\underset{1}{\bullet}\,\mathrm{d}\,\xi'\mathrm{d}\,\xi = Ft_D\,\mathrm{e}^{[w(0)-w(1)]/2}\int_0^1\int_\xi^1 \mathrm{e}^{w(\xi')-w(\xi)}d(\xi')^{-1}\mathrm{d}\,\xi'\mathrm{d}\,\xi. \tag{54}$$

4.3. The generalized King–Altman dictionary

We have constructed a list of diagrams, involving the interval $[0,1]$, used to find the steady-state solutions of the three framework models discussed below:

$$\underset{0}{\bullet}\xrightarrow{\quad}\underset{1}{\bullet} = \gamma = F\,\mathrm{e}^{[w(0)-w(1)]/2}, \tag{55}$$

$$\underset{0}{\bullet}\xleftarrow{\quad}\underset{1}{\bullet} = \delta = F\,\mathrm{e}^{[w(1)-w(0)]/2}, \tag{56}$$

$$\underset{0}{\bullet}\xrightarrow{\quad}\underset{\xi}{|}\xleftarrow{\quad}\underset{1}{\bullet} = F\,\mathrm{e}^{[w(0)-2w(\xi)+w(1)]/2}, \tag{57}$$

$$\underset{0}{\bullet}\xleftarrow{\quad}\underset{\xi'}{|}\xrightarrow{\quad}\underset{1}{\bullet} = Ft_D n^{-2}\,\mathrm{e}^{-[w(0)-2w(\xi')+w(1)]/2}d(\xi')^{-1}, \tag{58}$$

$$\int_0^1 \underset{0}{\bullet}\xrightarrow{\quad}\underset{\xi}{|}\xrightarrow{\quad}\underset{1}{\bullet}\,\mathrm{d}\,\xi = Fn\,\mathrm{e}^{[w(0)+w(1)]/2}g, \tag{59}$$

$$\int_0^1 \underset{0}{\bullet}\xrightarrow{\quad}\underset{\xi'}{|}\xrightarrow{\quad}\underset{1}{\bullet}\,\mathrm{d}\,\xi' = Ft_D n^{-1}\,\mathrm{e}^{-[w(0)+w(1)]/2}h(1), \tag{60}$$

$$\int_\xi^1 \underset{0}{\bullet}\xrightarrow{\quad}\underset{\xi}{|}\xrightarrow{\quad}\underset{\xi'}{|}\xrightarrow{\quad}\underset{1}{\bullet}\,\mathrm{d}\,\xi' = Ft_D n^{-1}\,\mathrm{e}^{[w(0)-2w(\xi)-w(1)]/2}[h(1)-h(\xi)], \tag{61}$$

$$\int_0^\xi \underset{0}{\bullet}\xrightarrow{\quad}\underset{\xi'}{|}\xrightarrow{\quad}\underset{\xi}{|}\xrightarrow{\quad}\underset{1}{\bullet}\,\mathrm{d}\,\xi' = Ft_D n^{-1}\,\mathrm{e}^{[w(1)-2w(\xi)-w(0)]/2}h(\xi), \tag{62}$$

$$\int_0^1\int_\xi^1 \underset{0}{\bullet}\xrightarrow{\quad}\underset{\xi}{|}\xrightarrow{\quad}\underset{\xi'}{|}\xrightarrow{\quad}\underset{1}{\bullet}\,\mathrm{d}\,\xi'\,\mathrm{d}\,\xi = Ft_D\,\mathrm{e}^{[w(0)-w(1)]/2}[h(1)g-i], \tag{63}$$

$$\int_0^1\int_0^\xi \underset{0}{\bullet}\xrightarrow{\quad}\underset{\xi'}{|}\xrightarrow{\quad}\underset{\xi}{|}\xrightarrow{\quad}\underset{1}{\bullet}\,\mathrm{d}\,\xi'\,\mathrm{d}\,\xi = Ft_D\,\mathrm{e}^{[w(1)-w(0)]/2}i. \tag{64}$$

These diagrams involve the following three integrals:

$$h(\xi) = \int_0^{\xi} \mathrm{e}^{w(\xi')} d(\xi')^{-1}\, \mathrm{d}\,\xi', \tag{65}$$

$$g = \int_0^1 \mathrm{e}^{-w(\xi)}\, \mathrm{d}\,\xi, \tag{66}$$

$$i = \int_0^1 \int_0^{\xi} \mathrm{e}^{w(\xi')-w(\xi)} d(\xi')^{-1}\, \mathrm{d}\,\xi'\, \mathrm{d}\,\xi = \int_0^1 h(\xi)\, \mathrm{e}^{-w(\xi)}\, \mathrm{d}\,\xi. \tag{67}$$

Integrated diagrams are obtained as limits of Riemann sums. Formally, to pass from a diagram to a corresponding integrated diagram, the expression to the right is multiplied by n and integrated with respect to the independent variable. Diagrams (55) and (56) are special cases of diagram (57) for $\xi = 1$ and $\xi = 0$, respectively. Diagram (61) $\rightarrow$ diagram (60) as $\xi \rightarrow 0$ and diagram (62) $\rightarrow$ diagram (60) as $\xi \rightarrow 1$.

5. Solution of the single-particle model

5.1. *Exponential boundary conditions*

In this section, we apply the generalized King–Altman method to analyze the single-particle model at steady state. Begin with the general case of exponential boundary conditions, which are constructed by using the entrance and exit rates defined by Eqs. (3)–(6). The probability that the pore is empty is proportional to the sum over all diagrams directed towards the empty state:

$\mathcal{D}Q_E =$ 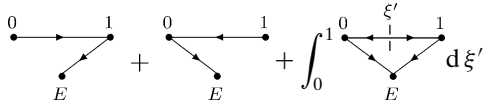 $\mathrm{d}\,\xi'$

$$= \gamma\beta_{\mathrm{II}} + \delta\beta_{\mathrm{I}} + \beta_{\mathrm{I}}\beta_{\mathrm{II}} \int_0^1 \quad \mathrm{d}\,\xi', \tag{68}$$

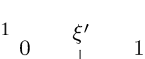

where $\mathcal{D}$ is the sum of all directed diagrams. Note from Eqs. (3)–(6) and the dictionary that each term is proportional to Fn. The probability that an ion in the pore occupies the interval $[\xi, \xi + \Delta\xi]$ for $\xi \in [0, 1 - \Delta\xi]$ is obtained by summing over all diagrams directed towards ξ.

$\mathcal{D}Q(\xi) = \mathcal{D}p(\xi)\Delta\xi$

$=$ 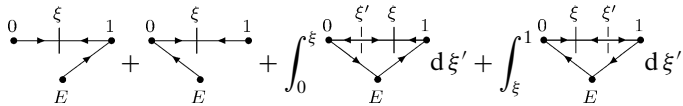

$$= \alpha_{\mathrm{II}} c_{\mathrm{II}}$$ 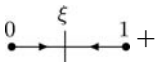 $$+ \alpha_{\mathrm{I}} c_{\mathrm{I}}$$ 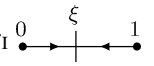 $$+ \beta_{\mathrm{I}} \alpha_{\mathrm{II}} c_{\mathrm{II}} \int_0^{\xi}$$ 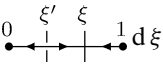 $$\mathrm{d}\,\xi'$$

$$+ \beta_{\mathrm{II}} \alpha_{\mathrm{I}} c_{\mathrm{I}} \int_{\xi}^{1}$$ 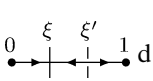 $$\mathrm{d}\,\xi'. \tag{69}$$

$p(\xi)$ is the probability density of ion occupation. Inspection of Eqs. (3)–(6) and the dictionary shows that $\mathcal{D}Q(\xi) \propto F$ and $\mathcal{D}p(\xi) \propto Fn$. The probability that an ion occupies the pore is proportional to

$$\mathcal{D} \int_0^1 p(\xi)\,\mathrm{d}\,\xi = (\alpha_{\mathrm{I}} c_{\mathrm{I}} + \alpha_{\mathrm{II}} c_{\mathrm{II}}) \int_0^1$$ 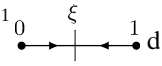 $$\mathrm{d}\,\xi$$

$$+ \beta_{\mathrm{I}} \alpha_{\mathrm{II}} c_{\mathrm{II}} \int_0^1 \int_0^{\xi}$$ 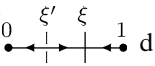 $$\mathrm{d}\,\xi'\,\mathrm{d}\,\xi$$

$$+ \beta_{\mathrm{II}} \alpha_{\mathrm{I}} c_{\mathrm{I}} \int_0^1 \int_{\xi}^1$$ 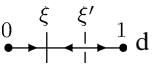 $$\mathrm{d}\,\xi'\,\mathrm{d}\,\xi. \tag{70}$$

Each term is proportional to Fn. Since probability on the state diagram is normalized, we have

$$\mathcal{D} = \mathcal{D}Q_E + \mathcal{D} \int_0^1 p(\xi)\,\mathrm{d}\,\xi. \tag{71}$$

Dividing Eqs. (68) and (69) by $\mathcal{D}$, we obtain expressions for Q_E and $p(\xi)$ that are independent of n.

In the ordinary King–Altman method the net flux J flowing clockwise around a cycle is given by the cyclic diagram flowing clockwise around the cycle minus the cyclic diagram flowing counterclockwise (Hill, 1977). Equation (36) gives an example. This property is inherited by the generalized King–Altman method as can be seen by considering the limit $n \to \infty$ of a difference between cyclic diagrams. For the case of the single-particle model

$$\mathcal{D}J =$$ 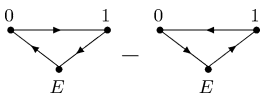

$$= \alpha_{\mathrm{I}} c_{\mathrm{I}} \gamma \beta_{\mathrm{II}} - \alpha_{\mathrm{II}} c_{\mathrm{II}} \delta \beta_{\mathrm{I}}. \tag{72}$$

An expression for J is obtained when this result is divided by $\mathcal{D}$. A standard analytical formula may be developed by dividing Eq. (72) by (71), substituting for the transition rates using Eqs. (1)–(6), and expanding the diagrams in Eqs. (68) and (70) using the dictionary developed in Section 4.3. For the case of a constant diffusion coefficient, $d(\xi) \equiv 1$, the result agrees with the expressions obtained by direct integration (McGill and Schumaker, 1996; Schumaker, 2002).

5.2. Confirmation of the solution

The framework model for single-particle conduction solves the time-independent Smoluchowski Eq. (12) with boundary conditions, Eqs. (16) and (17), and the

normalization condition, Eq. (18). It is easy to verify directly that the solution we have constructed using the generalized King–Altman method satisfies these equations.

First, note that the normalization condition, Eq. (18), is satisfied by construction, since Eq. (71) is used to define $\mathcal{D}$. We next consider whether $p(\xi)$ as defined by Eq. (69) satisfies the Smoluchowski equation. But this expression is a linear combination of diagrams (57), (61), and (62). Diagram (57) is proportional to the Boltzmann density $\exp(-w(\xi))$ which is the solution of the Smoluchowski equation at thermodynamic equilibrium (corresponding to $J = 0$ in the Nernst–Planck Eq. (13)). Diagrams (61) and (62) include terms proportional to the Boltzmann density or $\exp(-w(\xi))h(\xi)$. Differentiation of this latter expression verifies that it is also a solution of the Smoluchowski equation. It follows that the expression for $p(\xi)$ constructed by the King–Altman method satisfies the Smoluchowski equation.

It remains to be seen that the boundary conditions are satisfied. Consider the boundary condition on side I, Eq. (16). Solve for J, multiply by $\mathcal{D}$, and then express the coefficients of $\mathcal{D}Q_E$ and $\mathcal{D}p(0)$ in terms of the proton entrance and exit rates using Eqs. (3) and (4). Obtain

$$\mathcal{D}J = \mathcal{D}Q_E\alpha_{\mathrm{I}}c_{\mathrm{I}} - \mathcal{D}p(0)\Delta\xi\beta_{\mathrm{I}}. \tag{73}$$

Direct substitution on the right-hand side using Eqs. (68) and (69), with $\xi \to 0$, followed by cancellation of terms yields the expression on the right-hand side of Eq. (72). This shows that the solution constructed using the King–Altman method satisfies Eq. (16). An analysis of the boundary condition on side II, Eq. (17), is similar.

5.3. Levitt boundary conditions

The entrance and exit rates corresponding to Levitt boundary conditions are obtained by multiplying the right-hand sides of Eqs. (3)–(6) by n. Transition rates in the interval $0 \le \xi \le 1$ are still given by Eqs. (1) and (2). As a result, only the last term on the right-hand side of Eq. (68) and only the last two terms on the right-hand side of Eq. (70) are of dominant order in n:

$$\mathcal{D}Q_E = \beta_{\mathrm{I}}\beta_{\mathrm{II}} \int_0^1 \; \underset{0}{\bullet}\!\!\longleftarrow\!\!\underset{\xi'}{|}\!\!\longrightarrow\!\!\underset{1}{\bullet}\; \mathrm{d}\,\xi' + o(Fn^3), \tag{74}$$

$$\mathcal{D}\int_0^1 p(\xi)\,\mathrm{d}\,\xi = \beta_{\mathrm{I}}\alpha_{\mathrm{II}}c_{\mathrm{II}} \int_0^1 \int_0^{\xi} \; \underset{0}{\bullet}\!\!\longleftarrow\!\!\underset{\xi'}{|}\!\!\longrightarrow\!\!\underset{\xi}{|}\!\!\longleftarrow\!\!\underset{1}{\bullet}\; \mathrm{d}\,\xi'\,\mathrm{d}\,\xi$$

$$+ \beta_{\mathrm{II}}\alpha_{\mathrm{I}}c_{\mathrm{I}} \int_0^1 \int_{\xi}^1 \; \underset{0}{\bullet}\!\!\longrightarrow\!\!\underset{\xi}{|}\!\!\longleftarrow\!\!\underset{\xi'}{|}\!\!\longrightarrow\!\!\underset{1}{\bullet}\; \mathrm{d}\,\xi'\,\mathrm{d}\,\xi + o(Fn^3), \tag{75}$$

where $o(Fn^3)$ denotes terms of higher order in n^{-1} than Fn^3. When J is calculated as a ratio by dividing the right-hand side of Eq. (72) by $\mathcal{D}$ and letting $n \to \infty$, only the terms given explicitly on the right-hand sides of Eqs. (74) and (75) survive in the denominator. For the case of constant diffusion, the result agrees with that obtained by direct integration (Levitt, 1986; Schumaker, 2002).

6. Solution of the Grotthuss conduction model

6.1. Construction of the solution

In this section, we solve the Grotthuss conduction model, Eqs. (28)–(33), using the generalized King–Altman method. The state diagram is shown by Fig. 5(a). The model is constructed as the $n \to \infty$ limit of the random walk shown in Fig. 5(b). Calculation reveals that directed diagrams of that random walk whose missing transition links a lumped state with the empty segment have one less factor of n than other directed diagrams. After dividing through by $\mathcal{D}$ and letting $n \to \infty$, their contribution goes to zero. These diagrams have open circles signifying lumped states in expressions given later. For simplicity, their contributions are neglected in the expressions that follow them. Site indices increase to the left on the empty segment (Fig. 5(b)). Thus, for example, γ^E involves a product of transitions to the left. Once the diagram expressions are expressed as products of transition rates and dictionary entries, the empty segment terms are oriented left to right, consistent with the dictionary. To reduce clutter, the labeling of values $\xi^{s\prime}$ that arrows diverge from (marked by dashed cuts through diagrams), and values ξ^s that arrows converge to (marked by solid cuts through diagrams), have been omitted from built-up diagram expressions.

To begin the development of diagram expressions, the probability of being in the lumped state on side I is

$\mathcal{D}Q^b_{\rm I} =$ 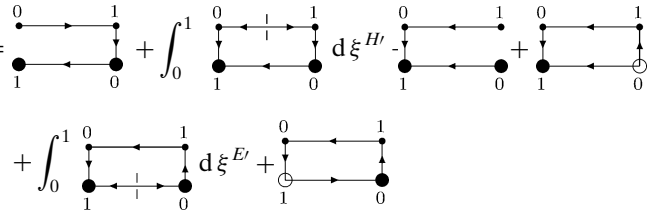 (76)

$= \gamma^H \beta_{\rm II}\eta_{\rm II}\gamma^E \nu_{\rm I} + \beta_{\rm I}\beta_{\rm II}\eta_{\rm II}\gamma^E\nu_{\rm I}\int_0^1 \xi^{H\prime}\,{\rm d}\xi^{H\prime} + \delta^H\beta_{\rm I}\eta_{\rm II}\gamma^E\nu_{\rm I}$

$+ \nu_{\rm II}\alpha_{\rm II}c_{\rm II}\delta^H\beta_{\rm I}\nu_{\rm I}\int_0^1 \xi^{E\prime}\,{\rm d}\xi^{E\prime} + o(F_H F_E n^4),$ (77)

where $F_s, s \in \{H, E\}$ is given by Eq. (39) with $t_D \to t_s$ and $d_{i,i+1} \to d^s_{i,i+1}$. The probability of being in the lumped state on side II is

$\mathcal{D}Q^b_{\rm II} =$ 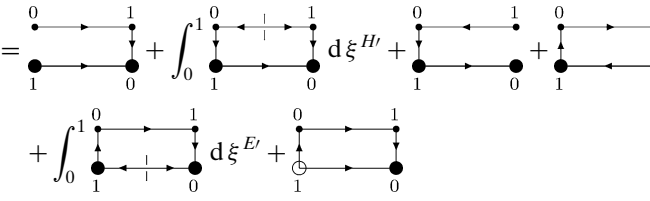 (78)

$$= \gamma^H \beta_{\mathrm{II}} \eta_{\mathrm{I}} \delta^E \nu_{\mathrm{II}} + \beta_{\mathrm{I}} \beta_{\mathrm{II}} \eta_{\mathrm{I}} \delta^E \nu_{\mathrm{II}} \int_0^1$$

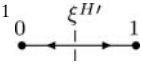

$$\mathrm{d}\,\xi^{H\prime} + \delta^H \beta_{\mathrm{I}} \eta_{\mathrm{I}} \delta^E \nu_{\mathrm{II}}$$

$$+ \nu_{\mathrm{I}} \alpha_{\mathrm{I}} c_{\mathrm{I}} \gamma^H \beta_{\mathrm{II}} \nu_{\mathrm{II}} \int_0^1$$

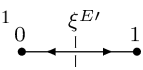

$$\mathrm{d}\,\xi^{E\prime} + o(F_H F_E n^4). \tag{79}$$

The probability of being in the proton interval $[\xi^H, \xi^H + \Delta\xi]$ for $\xi \in [0, 1 - \Delta\xi]$ is

$$\mathcal{D}Q^H(\xi^H) = \mathcal{D}p^H(\xi^H)\Delta\xi^H$$

$$=$$

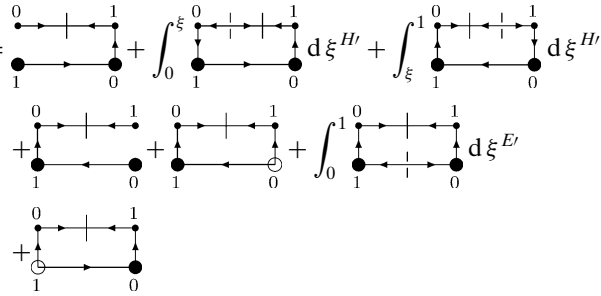

(80)

$$= \eta_{\mathrm{I}} \delta^E \nu_{\mathrm{II}} \alpha_{\mathrm{II}} c_{\mathrm{II}}$$

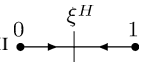

$$+ \beta_{\mathrm{I}} \eta_{\mathrm{I}} \delta^E \nu_{\mathrm{II}} \alpha_{\mathrm{II}} c_{\mathrm{II}} \int_0^{\xi^H}$$

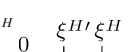

$$\mathrm{d}\,\xi^{H\prime} + \beta_{\mathrm{II}} \eta_{\mathrm{II}} \gamma^E \nu_{\mathrm{I}} \alpha_{\mathrm{I}} c_{\mathrm{I}} \int_{\xi^H}^1$$

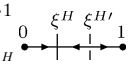

$$\mathrm{d}\,\xi^{H\prime} + \eta_{\mathrm{II}} \gamma^E \nu_{\mathrm{I}} \alpha_{\mathrm{I}} c_{\mathrm{I}}$$

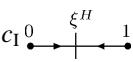

$$+ \nu_{\mathrm{II}} \alpha_{\mathrm{II}} c_{\mathrm{II}} \nu_{\mathrm{I}} \alpha_{\mathrm{I}} c_{\mathrm{I}}$$

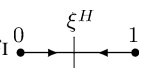

$$\int_0^1$$

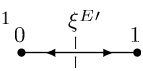

$$\mathrm{d}\,\xi^{E\prime} + o(F_H F_E n^3). \tag{81}$$

Notice that the last term given explicitly in Eq. (81) is proportional to the product $c_{\mathrm{I}} c_{\mathrm{II}}$. It arises from the second-to-last diagram in Eq. (80), which includes entrances on both sides I and II. This pair of entrances is due to the structured nature of the empty state. No such term arises in the expression for the denominator of the single-particle model because the empty state is a simple point in the state space. The probability of being in the empty interval $[\xi^E, \xi^E + \Delta\xi^E]$ for $\xi \in [0, 1 - \Delta\xi]$ is

$$\mathcal{D}Q^E(\xi^E) = \mathcal{D}p^E(\xi^E)\Delta\xi^E$$

$$=$$

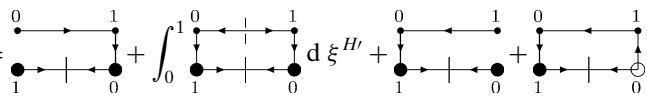

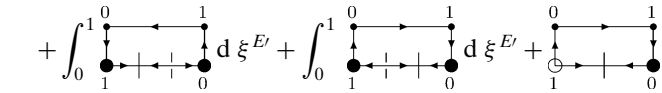

(82)

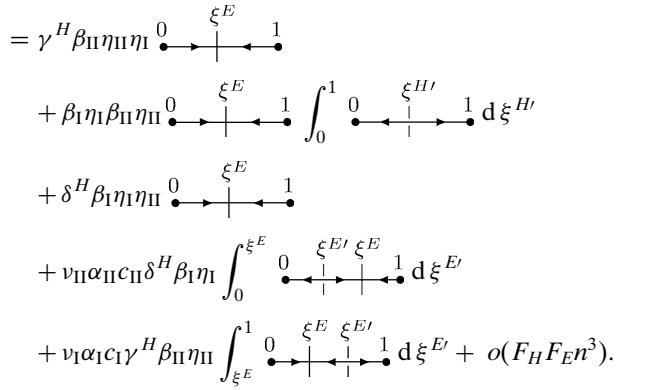

(83)

Finally, the net flux J is

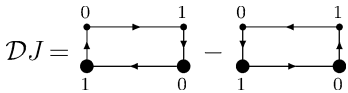

(84)

$$= \alpha_{\mathrm{I}} c_{\mathrm{I}} \gamma^H \beta_{\mathrm{II}} \eta_{\mathrm{II}} \gamma^E \nu_{\mathrm{I}} - \alpha_{\mathrm{II}} c_{\mathrm{II}} \delta^H \beta_{\mathrm{I}} \eta_{\mathrm{I}} \delta^E \nu_{\mathrm{II}}. \tag{85}$$

Again, $\mathcal{D}$ represents the sum of all directed diagrams,

$$\mathcal{D} = \mathcal{D} Q_{\mathrm{I}}^b + \mathcal{D} Q_{\mathrm{II}}^b + \mathcal{D} \int_0^1 p^H(\xi^H)\, \mathrm{d}\xi^H + \mathcal{D} \int_0^1 p^E(\xi^E)\, \mathrm{d}\xi^E. \tag{86}$$

Expressions for the probabilities, Q_{I}^b and Q_{II}^b, densities, $p^H(\xi)$ and $p^E(\xi)$, and current J can be obtained by substituting from the expressions for the transitions rates, Eqs. (19)–(27), and from the dictionary, Eqs. (55)–(63), dividing by $\mathcal{D}$, canceling a common factor in the numerator and denominator, and letting $n \to \infty$. Calculation of $\mathcal{D}$ involves integrating over the densities, and therefore replacing diagrams in Eqs. (81) and (83) by integrated diagrams. For example, diagrams defined by Eqs. (57), (61), and (62) are replaced by the integrated diagrams defined by Eqs. (59), (63), and (64), respectively.

The expression obtained for J agrees with the result of direct integration (Schumaker et al., 2001) when specialized to the case of constant diffusion coefficients and $f_N = 0$. Formulas for Q_{I}^b, Q_{II}^b, p^H, and p^E have not been published previously, even in a special case. The diagram method shows that expressions for all of these quantities have the form of ratios, with a common denominator. Even without forming the detailed expression for J, it is clear that it will have the form

$$J = (c_{\mathrm{I}} \mathrm{e}^{\psi_{\mathrm{I}}} - c_{\mathrm{II}})/(a_0 + a_1 c_{\mathrm{I}} + a_2 c_{\mathrm{II}} + a_3 c_{\mathrm{I}} c_{\mathrm{II}}), \tag{87}$$

where a_0, a_1, a_2, and a_3 are positive and do not depend on the excess proton concentrations, c_{I} and c_{II}, in the bulk. This shows that, under conditions of symmetrical concentrations, $c_{\mathrm{I}} = c_{\mathrm{II}} = c$, and for $\psi_{\mathrm{I}} > 0$ fixed, the current as a function of c has a maximum value for some $c = c_{\max} > 0$, and is concave down on an interval $(0, c_{\inf})$ that includes $c_{\max}$ in its interior. Therefore, the mechanism sketched in Fig. 4 can never account for the shoulder in the current data of Gowen et al. (2002). This insight limits the present Grotthuss mechanism to modeling proton conduction through gramicidin in the regime of low proton concentrations and supports the suggestion that the shoulder in the current data signifies the onset of a conduction mechanism in which the pore may be occupied by more than one excess proton.

6.2. *Confirmation of the solution*

The Grotthuss model solves the Smoluchowski equation (28) with the boundary conditions, Eqs. (29)–(32), and the normalization condition, Eq. (33). We now verify that the solution we have constructed by the generalized King–Altman method satisfies these equations. The solution is normalized by construction, since Eq. (86) is used to define $\mathcal{D}$. Furthermore, the Smoluchowski equations (28) are satisfied. The expressions for $p^H(\xi)$ and $p^E(\xi)$, proportional to Eqs. (81) and (83), are linear combinations of the diagrams (57), (61), and (62) (for $w = w^H$ and $w = w^E$, respectively). These diagrams individually satisfy the Smoluchowski equations, as described above in Section 5.2. Note that diagram (60) is independent of ξ.

It remains to be seen that the boundary conditions are satisfied. First, consider Eq. (29), which involves $p^E(1)$ and Q^b_{I}. From Eq. (83) we have

$$\begin{aligned}\mathcal{D}p^E(1)\Delta\xi = {} & \gamma^H\beta_{\mathrm{II}}\eta_{\mathrm{II}}\eta_{\mathrm{I}}\gamma^E + \beta_{\mathrm{I}}\eta_{\mathrm{I}}\beta_{\mathrm{II}}\eta_{\mathrm{II}}\gamma^E \int_0^1 \overset{0}{\bullet}\!\!\longleftarrow\!\!\overset{\xi^{H\prime}}{|}\!\!\longrightarrow\!\!\overset{1}{\bullet}\, \mathrm{d}\xi^{H\prime} \\ & + \delta^H\beta_{\mathrm{I}}\eta_{\mathrm{I}}\eta_{\mathrm{II}}\gamma^E + \nu_{\mathrm{II}}\alpha_{\mathrm{II}}c_{\mathrm{II}}\delta^H\beta_{\mathrm{I}}\eta_{\mathrm{I}} \int_0^1 \overset{0}{\bullet}\!\!\longleftarrow\!\!\overset{\xi^{E\prime}}{|}\!\!\longrightarrow\!\!\overset{1}{\bullet}\, \mathrm{d}\xi^{E\prime} \\ & + o(F_H F_E n^3). \end{aligned} \tag{88}$$

Terms of dominant order in n are proportional to η_{I} and, from Eq. (77), those terms in $\mathcal{D}Q^b_{\mathrm{I}}$ are proportional to ν_{I} with the same coefficient:

$$\mathcal{D}Q^b_{\mathrm{I}}/\nu_{\mathrm{I}} = \mathcal{D}p^E(1)\Delta\xi/\eta_{\mathrm{I}} + o(F_H F_E n^2). \tag{89}$$

Multiply by ν_{I}, substitute for $\nu_{\mathrm{I}}\Delta\xi/\eta_{\mathrm{I}}$ using Eqs. (25) and (26), divide by $\mathcal{D}$, and let $n \to \infty$ to obtain the boundary condition on side I, Eq. (29). The analysis of the boundary condition Eq. (30) is similar.

Next, consider the boundary condition Eq. (31). Solve for J and multiply by $\mathcal{D}$. The coefficients of $\mathcal{D}Q^b_{\mathrm{I}}$ and $\mathcal{D}p^H(0)$ can be expressed in terms of entrance and exit rates, using Eqs. (21) and (22), yielding

$$\mathcal{D}J = \mathcal{D}Q^b_{\mathrm{I}}\alpha_{\mathrm{I}}c_{\mathrm{I}} - \mathcal{D}p^H(0)\Delta\xi\beta_{\mathrm{I}}, \tag{90}$$

which is confirmed to leading order in n by substitution from Eqs. (77) and (81). This shows that Eq. (31) is satisfied in the limit $n \to \infty$. A similar analysis confirms boundary condition Eq. (32).

7. The diffusive shaking stack

7.1. The framework model

The Grotthuss model is an elaboration of the single-particle model. However, framework models of ion permeation can also be constructed for conduction mechanisms that involve more than one ion in the pore. The shaking stack model of ion conduction through the Ca^{2+}-activated K^+ channel (Schumaker, 1992) is a variant of the vacancy diffusion mechanism (Schumaker and MacKinnon, 1990). It was originally formulated as a random walk model, involving a cycle of states in which the pore is occupied by either $m-1$ or m ions. Molecular dynamics simulations have encountered a pathway for ion conduction through the KcsA K^+ channel that is similar to the shaking stack mechanism (pathway a–c–d–e–f in Fig. 2 of Bernèche and Roux, 2001), although more recent simulations that take into account an applied field prefer a knock-on mechanism (Bernèche and Roux, 2003). In addition, two sets of KcsA conductance data have been rationalized in terms of a very simple model (Nelson, 2002, 2003), which can be obtained from the shaking stack model in the limit that the translocation rate of the stack of $m-1$ ions becomes very rapid. This section generalizes the shaking stack model so that transport of the stack of $m-1$ ions is described diffusively, which is more realistic than the discontinuous hopping implicit in the random walk models.

The state diagram for a diffusive shaking stack model is given in Fig. 7(a). In general, this mechanism involves an isolated state of m ions (at the apex) coupled with a segment of $m-1$ ion states. The cartoons depict a triply occupied state T coupled with a segment of doubly occupied states D, consistent with X-ray evidence for ion occupancy of the pore of the KcsA K^+ channel (Morais-Cabral et al., 2001).

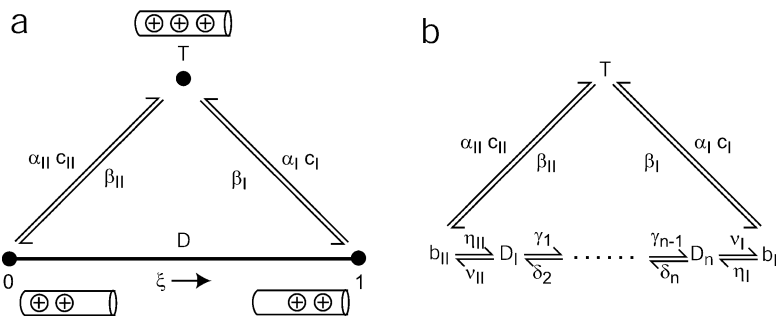

Fig. 7 (a) State diagram for the diffusive shaking stack model for $m = 3$. The triply occupied state T is coupled with the segment of doubly occupied states D. (b) Random walk used to construct the state diagram.

States at the ends of the D segment are lumped in order that the model includes exponentially distributed entrances into the T state. The rates of ion entrance are given by the same formulas, Eqs. (21) and (23), as for the Grotthuss model. The rates of ion exit from the triply occupied state are

$$\beta_{\mathrm{I}} = t_a^{-1}\,\mathrm{e}^{-f_X\psi_{\mathrm{I}}}, \tag{91}$$

$$\beta_{\mathrm{II}} = t_a^{-1}\,\mathrm{e}^{f_X\psi_{\mathrm{I}}}. \tag{92}$$

In contrast to Eqs. (22) and (24), these rates are not proportional to n. The exit rate is positive and finite in the limit $n \to \infty$ because exit occurs from a point state of positive probability. Fig. 7(b) shows the random walk used to construct the shaking stack model. The transition rates for the component that converges to the doubly occupied segment are given by

$$\gamma_i = t_D^{-1} n^2 d_{i,i+1}\,\mathrm{e}^{[w(\xi_i)-w(\xi_{i+1})]/2}, \tag{93}$$

$$\delta_i = t_D^{-1} n^2 d_{i,i-1}\,\mathrm{e}^{[w(\xi_i)-w(\xi_{i-1})]/2}, \tag{94}$$

$$\nu_{\mathrm{I}} = t_D^{-1} n^2 a\,\mathrm{e}^{f_B\psi_{\mathrm{I}}}, \tag{95}$$

$$\nu_{\mathrm{II}} = t_D^{-1} n^2 a\,\mathrm{e}^{-f_B\psi_{\mathrm{I}}}, \tag{96}$$

$$\eta_{\mathrm{I}} = \eta_{\mathrm{II}} = t_D^{-1} n. \tag{97}$$

These expressions are similar to those given by Eqs. (19), (20), and (25)–(27).

In the diffusion limit, the random walk between the doubly occupied states at the base of Fig. 7(b) converges to the Smoluchowski equation,

$$(d(\xi)p_D{}'(\xi))' + (d(\xi)w'(\xi)p_D(\xi))' = 0. \tag{98}$$

$p_D(\xi)$ is the probability density for the system to be in the doubly occupied state with reaction coordinate ξ, corresponding to a specific configuration of water molecules and two K^+ ions in the pore. The following boundary conditions are obtained

$$Q^b_{\mathrm{II}} = p_D(0)\,a\,\mathrm{e}^{-f_B\psi_{\mathrm{I}}}, \tag{99}$$

$$Q^b_{\mathrm{I}} = p_D(1)\,a\,\mathrm{e}^{f_B\psi_{\mathrm{I}}}. \tag{100}$$

Probability balance holds between the triply occupied state and the lumped states at each end of the doubly occupied segment, yielding the algebraic equation

$$Q_T(\beta_{\mathrm{I}} + \beta_{\mathrm{II}}) = Q^b_{\mathrm{I}}\alpha_{\mathrm{I}}c_{\mathrm{I}} + Q^b_{\mathrm{II}}\alpha_{\mathrm{II}}c_{\mathrm{II}}. \tag{101}$$

The probabilities and densities satisfy the normalization condition

$$Q_T + Q^b_{\mathrm{I}} + Q^b_{\mathrm{II}} + \int_0^1 p_D(\xi)\,\mathrm{d}\xi = 1. \tag{102}$$

Equations (98)–(102) give the framework model for the diffusive shaking stack.

7.2. Construction of the solution

Begin by calculating the common denominator $\mathcal{D}$. First consider $\mathcal{D}Q_T$, the sum of diagrams directed towards the triply occupied state T. Similar to the Grotthuss model, directed diagrams whose missing transition links a lumped state with the doubly occupied segment have one less factor of n than other directed diagrams, and their contribution vanishes in the limit $n \to \infty$.

$\mathcal{D}Q_T =$ 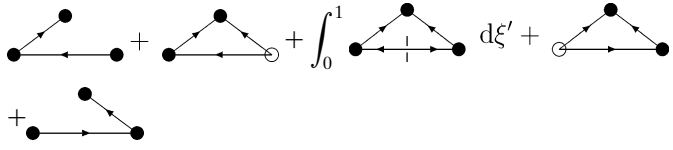

$= \eta_{\mathrm{I}}\delta\nu_{\mathrm{II}}\alpha_{\mathrm{II}}c_{\mathrm{II}} + \nu_{\mathrm{I}}\alpha_{\mathrm{I}}c_{\mathrm{I}}\nu_{\mathrm{II}}\alpha_{\mathrm{II}}c_{\mathrm{II}} \int_0^1$ 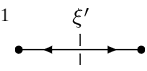 $\mathrm{d}\,\xi' + \eta_{\mathrm{II}}\gamma\nu_{\mathrm{I}}\alpha_{\mathrm{I}}c_{\mathrm{I}} + o(Fn^3).$

(103)

Notice that the second term of the last line is proportional to the product $c_{\mathrm{I}}c_{\mathrm{II}}$. The diagram expansion shows that this arises because of the structure of the doubly occupied state. The probabilities of the lumped states b_{I} and b_{II} are given by

$\mathcal{D}Q^b_{\mathrm{I}} = \int_0^1$ 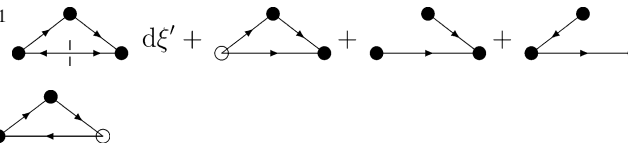

$= \nu_{\mathrm{II}}\alpha_{\mathrm{II}}c_{\mathrm{II}}\beta_{\mathrm{I}}\nu_{\mathrm{I}} \int_0^1$ 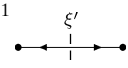 $\mathrm{d}\,\xi' + \beta_{\mathrm{I}}\nu_{\mathrm{I}}\gamma\eta_{\mathrm{II}} + \nu_{\mathrm{I}}\gamma\eta_{\mathrm{II}}\beta_{\mathrm{II}} + o(Fn^3),$

(104)

$\mathcal{D}Q^b_{\mathrm{II}} =$ 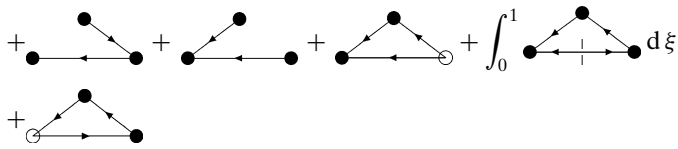

$= \beta_{\mathrm{I}}\eta_{\mathrm{I}}\delta\nu_{\mathrm{II}} + \eta_{\mathrm{I}}\delta\nu_{\mathrm{II}}\beta_{\mathrm{II}} + \nu_{\mathrm{II}}\beta_{\mathrm{II}}\alpha_{\mathrm{I}}c_{\mathrm{I}}\nu_{\mathrm{I}} \int_0^1$ 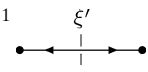 $\mathrm{d}\,\xi'$

$+ o(Fn^3).$ (105)

The probability of being in the doubly occupied interval $[\xi, \xi + \Delta\xi]$ for $\xi \in [0, 1 - \Delta\xi]$ is

$$\mathcal{D}Q(\xi) = \mathcal{D}p_D(\xi)\Delta\xi$$

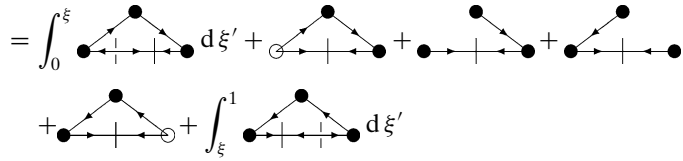

$$= \nu_{\mathrm{II}}\alpha_{\mathrm{II}}c_{\mathrm{II}}\beta_{\mathrm{I}}\eta_{\mathrm{I}} \int_0^{\xi}$$

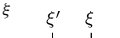

$$\mathrm{d}\,\xi' + (\beta_{\mathrm{I}} + \beta_{\mathrm{II}})\eta_{\mathrm{I}}\eta_{\mathrm{II}}$$

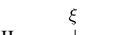

$$+ \nu_{\mathrm{I}}\alpha_{\mathrm{I}}c_{\mathrm{I}}\beta_{\mathrm{II}}\eta_{\mathrm{II}} \int_{\xi}^{1}$$

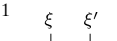

$$\mathrm{d}\,\xi' + o(Fn^2). \tag{106}$$

The common denominator $\mathcal{D}$ is given by the sum of all directed diagrams

$$\mathcal{D} = \mathcal{D}Q_T + \mathcal{D}Q_{\mathrm{I}}^b + \mathcal{D}Q_{\mathrm{II}}^b + \mathcal{D}\int_0^1 p_D(\xi)\,\mathrm{d}\,\xi, \tag{107}$$

where calculation of the integral involves integrating the diagrams on the last line of Eq. (106) with respect to ξ over the interval $[0, 1]$. The net flux J from side I to side II is proportional to the difference of cyclic diagrams:

$$\mathcal{D}J =$$

$$= \alpha_{\mathrm{I}}c_{\mathrm{I}}\beta_{\mathrm{I}}\eta_{\mathrm{II}}\gamma\nu_{\mathrm{I}} - \alpha_{\mathrm{II}}c_{\mathrm{II}}\beta_{\mathrm{II}}\eta_{\mathrm{I}}\delta\nu_{\mathrm{II}}. \tag{108}$$

An analytical formula can be obtained by expanding the diagrams in these expressions using the dictionary developed in Section 4.3. As with the Grotthuss model, the current has the form given by Eq. (87).

7.3. Confirmation of the solution

The solution is normalized by construction, since the denominator of all of the state probabilities is defined by multiplying Eq. (102) by $\mathcal{D}$ and then using Eqs. (103)–(105) and the integral of the terms given explicitly on the right-hand side of Eq. (106). The Smoluchowski equation is satisfied since the expression for $p_D(\xi)$, from Eq. (106), will be a linear combination of the dictionary diagrams defined by Eqs. (57), (61), and (62). Each of these components, separately, satisfy the Smoluchowski equation.

The boundary conditions for the Smoluchowski equation are also satisfied. Consider Eq. (99). From Eqs. (105) and (106), we find that

$$\mathcal{D}Q_{\mathrm{II}}^b/\nu_{\mathrm{II}} = \mathcal{D}p(0)\Delta\xi/\eta_{\mathrm{II}} + o(Fn). \tag{109}$$

Multiply by ν_{II}, substitute for $\nu_{\mathrm{II}}\Delta\xi/\eta_{\mathrm{II}}$ from Eqs. (96) and (97), divide by $\mathcal{D}$, and let $n \to \infty$ to obtain the boundary condition, Eq. (99). The boundary condition (100) can be confirmed similarly.

Finally, it is easy to see that Eq. (101) is satisfied. Multiply Eq. (103) by $\beta_{\mathrm{I}} + \beta_{\mathrm{II}}$, and Eq. (104) by $\alpha_{\mathrm{I}}c_{\mathrm{I}}$ and Eq. (105) by $\alpha_{\mathrm{II}}c_{\mathrm{II}}$. Substitute the resulting right-hand sides into Eq. (101), divide by $\mathcal{D}$, and let $n \to \infty$ to show that the algebraic equation is satisfied.

8. Summary and conclusion

Framework models are relatively simple stochastic models designed to incorporate potentials of mean force and diffusion coefficients calculated from detailed molecular simulations of biomolecules. They have been developed to bridge the gap in time scales between computer simulations and conductance measurements (McGill and Schumaker, 1996; Schumaker et al., 2000, 2001; Gowen et al., 2002; Bernèche and Roux, 2003). Even when the advance in computer technology overcomes the gap, framework models may remain useful as simple conceptual models of the dynamics described by the simulations.

This article constructs three framework models of ion permeation through membrane channels as the diffusion limit of random walks. The constructions obtain boundary conditions that enforce constraints on ion occupancy in the channel pores. In the single-particle and Grotthuss models, at most a single permeant ion occupies the pore. In the KcsA potassium channel model of Bernèche and Roux (2003), either two or three ions can occupy the permeation pore. In the diffusive shaking stack model, introduced in this paper, ion occupancy is limited to either $m-1$ or m ions in the pore.

Random walks are also used in traditional models of enzyme kinetics (King and Altman, 1956; Hill, 1977). The King–Altman method is a diagrammatic procedure developed by enzyme kineticists to compute and analyze steady-state solutions of those random walks, and is very convenient when the random walk state diagrams have only one or two cycles of states. We have applied the King–Altman method to sequences of random walks with only one cycle and converging to diffusions, and obtained a generalized method for calculating solutions of the systems of ordinary differential equations and algebraic equations that are the limits of the random walks. With the dictionary of diagram components that we have developed, the generalized King–Altman method can be much easier to implement than direct integration of these systems.

We have applied the generalized King–Altman method to an analysis of the single-particle model, the Grotthuss model, and a diffusive generalization of the shaking stack model. The method obtains the analytical solution of the Grotthuss model much more rapidly than direct integration and also reveals that rate limiting degrees of freedom of the empty pore state are responsible for the predicted decrease in proton conductance at very high symmetrical concentrations in the surrounding solution. This paper has also introduced a new framework model, the diffusive shaking stack model. Ion conductance is again predicted to decrease at very high symmetrical concentration of permeant ion in the surrounding solutions,

and the generalized King–Altman method shows that this is due to rate limiting degrees of freedom of the $m-1$ state.

A comparison can be made between random walk models of ion permeation, which have been popular in ion channel biophysics since the early 1970s (Heckmann and Vollmerhaus, 1970; Läuger, 1973), and the framework models described here. Random walk models approximate the state space of a system by a discrete set of points. They have the very great virtue of simplicity. When describing transitions over sufficiently high potential barriers and between well-defined potential wells, they can approximate diffusion (Kramers, 1940). A frequent difficulty with random walk models lies in determining physically significant values for a large number of free parameters. Framework models are generalizations of the random walk models: They approximate the state space of a system by a collection of line segments and points. The states of the system on the line segments evolve according to Smoluchowski equations, which approximate the generalized Langevin equations obtained by the projection of high-dimensional Hamiltonian dynamics to one coordinate. As we obtain exact solutions to the diffusion equations, our approach does not require that the potential have well-defined barriers or wells. For example, in the framework model for proton conduction through gramicidin, the proton occupied state has no potential barrier and only a shallow well (Fig. 4(b)). The potentials of mean force and diffusion coefficients of the Smoluchowski equation may be obtained from molecular dynamics simulations, reducing the number of free parameters in these models.

These results are limited to framework models that can be parameterized by a single reaction coordinate. Recently, several potentials of mean force have been calculated as a function of two or three reaction coordinates (Bernèche and Roux, 2001, 2003; Yu et al., 2003; Cohen and Schulten, 2004). Schumaker and Watkins (2004) construct a single-particle model with two reaction coordinates. The methods they use can be adapted to construct other models in two reaction coordinates and generalization to three reaction coordinates appears to be straightforward. Generally, these models must be solved numerically. However, in some cases the reaction dynamics seem to follow quasi-one-dimensional pathways within the higher dimensional state spaces (Bernèche and Roux, 2001, 2003; Cohen and Schulten, 2004). It may be that effective one-dimensional state spaces can be constructed for such systems and the generalized King–Altman method applied to analyze the resulting permeation models.

References

Agmon, N., 1995. The Grotthuss mechanism. Chem. Phys. Lett. 244, 456–462.

Agmon, N., Hopfield, J.J., 1983. Transient kinetics of chemical reactions with bounded diffusion perpendicular to the reaction coordinate: Intramolecular processes with slow conformational changes. J. Chem. Phys. 78(11), 6947–6959.

Allen, T.W., Chung, S.H., 2001. Brownian dynamics study of an open-state KcsA potassium channel. Biochim. Biophys. Acta 1515, 83–91.

Apaydin, M.S., Brutlag, D.L., Guestrin, C., Hsu, D., Latombe, J.-C., 2003. Stochastic roadmap simulation: An efficient representation and algorithm for analyzing molecular motion. J. Comput. Biol. 10, 257–281.

Arseniev, A.S., Barsukov, I.L., Bystrov, V.F., Lomize, A.L., Ovchinnikov, Y.A., 1985. ^{1}H-NMR study of gramicidin A transmembrane ion channel. Head-to-head right-handed, single-stranded helices. FEBS Lett. 186, 168–174.

Berne, B.J., Pecora, R., 1976. Dynamic Light Scattering. Wiley, New York.

Bernèche, S., Roux, B., 2001. Energetics of ion conduction through the K^+ channel. Nature 414, 73–76.

Bernèche, S., Roux, B., 2003. A microscopic view of conduction through the streptomyces lividans K^+ channel. Proc. Natl. Acad. Sci. U.S.A. 100, 8644–8648.

Chen, D., Lear, J., Eisenberg, B., 1997. Permeation through an open channel: Poisson-Nernst-Planck theory of a synthetic ionic channel. Biophys. J. 72, 97–116.

Chiu, S.W., Novotny, J.A., Jakobsson, E., 1993. The nature of ion and water barrier crossings in a simulated ion channel. Biophys. J. 64, 98–109.

Cohen, J., Schulten, K., 2004. Mechanism of anionic conduction across ClC. Biophys. J. 86, 836–845.

Crouzy, S., Woolf, T.B., Roux, B., 1994. A molecular dynamics study of gating in dioxolane-linked gramicidin A channels. Biophys. J. 67, 1370–1386.

Eisenman, G., Enos, B., Hagglund, J., Sandbloom, J., 1980. Gramicidin as an example of a single-filing ionic channel. Ann. N.Y. Acad. Sci. 339, 8–20.

Finkelstein, A., Andersen, O.S., 1981. The gramicidin A channel: A review of its permeability characteristics with special reference to the single-file aspect of transport. J. Membr. Biol. 59, 155–171.

Gowen, J.A., Markham, J.C., Morrison, S.E., Cross, T.A., Busath, D.D., Mapes, E.J., Schumaker, M.F., 2002. The role of Trp side chains in tuning single proton conduction through gramicidin channels. Biophys. J. 83, 880–898.

Grote, R.F., Hynes, J.T., 1980. The stable states picture of chemical reactions II. Rate constants for condensed and gas phase reaction models. J. Chem. Phys. 73, 2715–2732.

Heckmann, K., Vollmerhaus, W., 1970. Zur theorie der "single-file" diffusion. Z. Physik 71, 320–328.

Hill, T.L., 1977. Free Energy Transduction in Biology. Academic, New York.

Hille, B., 1992. Ionic Channels of Excitable Membranes. Sinauer, Sunderland, MA.

Ketcham, R.R., Roux, B.B., Cross, T.A., 1997. High-resolution polypeptide structure in a lamellar phase lipid environment from solid state NMR derived orientational constraints. Structure 5, 1655–1669.

King, E.L., Altman, C., 1956. A schematic method of deriving the rate laws for enzyme-catalyzed reactions. J. Phys. Chem. 60, 1375–1378.

Kramers, H.A., 1940. Brownian motion in a field of force. Physica 7, 284–304.

Läuger, P., 1973. Ion transport through pores, a rate-theory analysis. Biochim. Biophys. Acta 311, 423–441.

Levitt, D.G., 1986. Interpretation of biological ion channel flux data: Reaction rate versus continuum theory. Ann. Rev. Biophys. Biophys. Chem. 15, 29–57.

Mapes, E., Schumaker, M.F., 2001. Mean first passage times across a potential barrier in the lumped state approximation. J. Chem. Phys. 114, 76–83.

Mashl, R.J., Tang, Y., Schnitzer, J., Jakobsson, E., 2001. Hierarchical approach to predicting permeation in ion channels. Biophys. J. 81, 2473–2483.

McGill, P., Schumaker, M.F., 1996. Boundary conditions for single-ion diffusion. Biophys. J. 71, 1723–1742.

Morais-Cabral, J.H., Zhou, Y., MacKinnon, R., 2001. Energetic optimization of ion conduction rate by the K^+ selectivity filter. Nature 414, 37–42.

Mori, H., 1965. Transport, collective motion and Brownian motion. Prog. Theor. Phys. 33, 423–455.

Nadler, B., Naeh, T., Schuss, Z., 2001. The stationary arrival process of independent diffusers from a continuum to an absorbing boundary is poissonian. SIAM J. Appl. Math. 62(2), 433–447.

Nelson, P.H., 2002. A permeation theory for single-file ion channels: Corresponding occupancy states produce Michaelis– Menten behavior. J. Chem. Phys. 117(24), 11396–11403.

Nelson, P.H., 2003. Modeling the concentration-dependent permeation modes of the KcsA potassium ion channel. Phys. Rev. E 68(061908).

Pomès, R., Roux, B., 1996. Structure and dynamics of a proton wire: A theoretical study of H^+ translocation along the single-file water chain in the gramicidin a channel. Biophys. J. 71, 19–39.
Pomès, R., Roux, B., 2002. Molecular mechanism of H^+ conduction in the single-file water chain of the gramicidin channel. Biophys. J. 82, 2304–2316.
Roux, B., 2002. Theoretical and computational models of ion channels. Curr. Opin. Struct. Biol. 12, 182–189.
Roux, B., Allen, T., Bernèche, S., Im, W., 2004. Theoretical and computational models of biological ion channels. Q. Rev. Biophys. 37, 15–103.
Roux, B., Karplus, M., 1993. Ion transport in the gramicidin channel: Free energy of the solvated right-hand dimer in a model membrane. J. Am. Chem. Soc. 115, 3250–3262.
Schumaker, M.F., 1992. Shaking stack model of ion conduction through the Ca^{2+}-activated K^+ channel. Biophys. J. 63, 1032–1044.
Schumaker, M.F., 2002. Boundary conditions and trajectories of diffusion processes. J. Chem. Phys. 116(6), 2469–2473.
Schumaker, M.F., 2003. Numerical framework models of single-proton conduction through gramicidin. Front. Biosci. 8, s982–s991.
Schumaker, M.F., MacKinnon, R., 1990. A simple model for multi-ion permeation. Biophys. J. 58, 975–984.
Schumaker, M.F., Pomès, R., Roux, B., 2000. A combined molecular dynamics and diffusion model of single proton conduction through gramicidin. Biophys. J. 79, 2840–2857.
Schumaker, M.F., Pomès, R., Roux, B., 2001. A framework model for single proton conductance through gramicidin. Biophys. J. 80, 12–30.
Schumaker, M.F., Watkins, D.S., 2004. A framework model based on the Smoluchowski equation in two reaction coordinates. J. Chem. Phys. 121, 6134–6144.
Tolokh, I.S., White, G.W.N., Goldman, S., Gray, C.G., 2002. Prediction of ion channel transport from Grote-Hynes and Kramers theories. Mol. Phys. 100, 2351–2359.
Tripathi, S., Hladky, S.B., 1998. Streaming potentials in gramicidin channels measured with ion-selective microelectrodes. Biophys. J. 74, 2912–2917.
Tuckerman, M.E., Berne, B.J., 1991. Stochastic molecular dynamics in systems with multiple timescales and memory friction. J. Chem. Phys. 95, 4389–4396.
Yin, H.-M., 2004. On a class of parabolic equations with nonlocal boundary conditions. J. Math. Anal. Appl. 294, 712–728.
Yu, C.-H., Cukierman, S., Pomès, R., 2003. Theoretical study of the structure and dynamic fluctuations of dioxolane-linked gramicidin channels. Biophys. J. 84, 816–831.
Zhou, M., MacKinnon, R., 2004. A mutant KcsA K^+ channel with altered conduction properties and selectivity filter ion distribution. J. Mol. Biol. 338, 839–846.
Zwanzig, R., 2001. Nonequilibrium Statistical Mechanics. Oxford University Press, New York.
Zwanzig, R.W., 1961. Statistical mechanics of irreversibility. In: Brittin, W.E., Downs, B.W., Downs, J. (Eds.), Lectures in Theoretical Physics, vol. 3. Interscience, New York, pp. 106–141.